# Irrigation - Appendix

## Collection 9

**General coordinator**
Eliseu Weber

**Team**
Kênia Samara Mourão Santos
Paulo Domingos Pires Teixeira Junior

## 1 Overview of the classification method

The MapBiomas project produces, among other land use and land cover classes, annual irrigation agriculture maps in Brazil from 1985 to the present. The first irrigation agriculture map from MapBiomas was released on Collection 5, comprising from 2000 to 2019, with maps of center pivot irrigation, covering all Brazil, and other irrigation systems, covering only the semiarid region. In Collection 6, the irrigation rice class was added and the other classes were extended to the 1985-2020 period. In Collection 7.1, in addition with the classes from the previous Collections, was added a new type of information about irrigation, the pivot dynamic. Pivot dynamics consists in presenting individualized characteristics of each pivot, such as number of cycles per year, dates of start and end cycles, and average daily precipitation. In the Collection 8 and Collection 9, the information about center pivot, other irrigation systems and pivot dynamics were reviewed and the 2022 and 2023 years were added, respectively. Figure 1 presents the evolution of irrigation agriculture classes within the MapBiomas project.

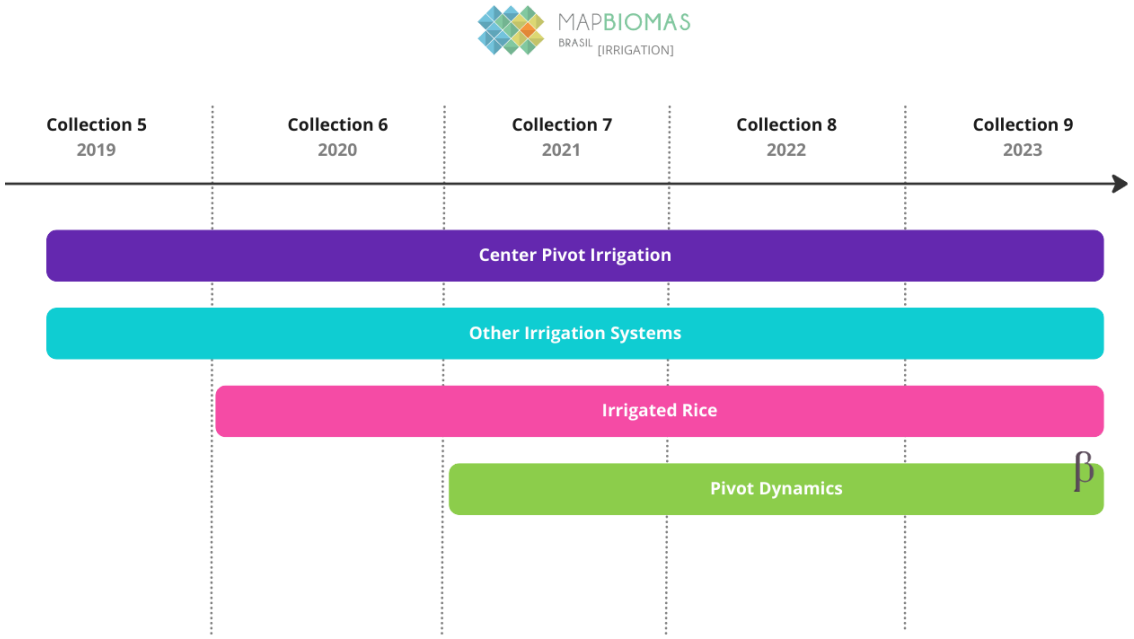


**Figure 1**: Comparison between the ‘ Irrigation Agriculture’ classes of MapBiomas Collection 5, 6, 7.1, 8 and 9. The pivot dynamics products are still in beta.

## 2 Center pivot irrigation systems

The first attempts in the MapBiomas project for mapping center pivot irrigation systems came through the Next Generation Mapping (NexGenMap) project. The objective of this initiative was to develop machine learning algorithms, tools and methods for producing the most current, detailed and accurate maps of land use and land cover using daily PlanetScope imagery, cloud computing, and new artificial intelligence algorithms. In the NextGenMap

project, artificial intelligence algorithms were developed to map center pivot irrigation systems using PlanetScope imagery in the Cerrado biome (SARAIVA et al., 2020).

In MapBiomas context, the mapping of 'Center pivot irrigation systems' was performed using Landsat imagery and an adapted U-Net architecture (RONNEBERGER et al., 2015), an image segmentation convolutional neural network architecture. The adapted U-Net architecture was trained with two different sets of samples, one set with center pivot irrigation systems samples and other with irrigated rice samples. To increase the temporal and spatial consistency of the final maps, the raw result was post-processed using temporal and spatial filters (Figure 2).

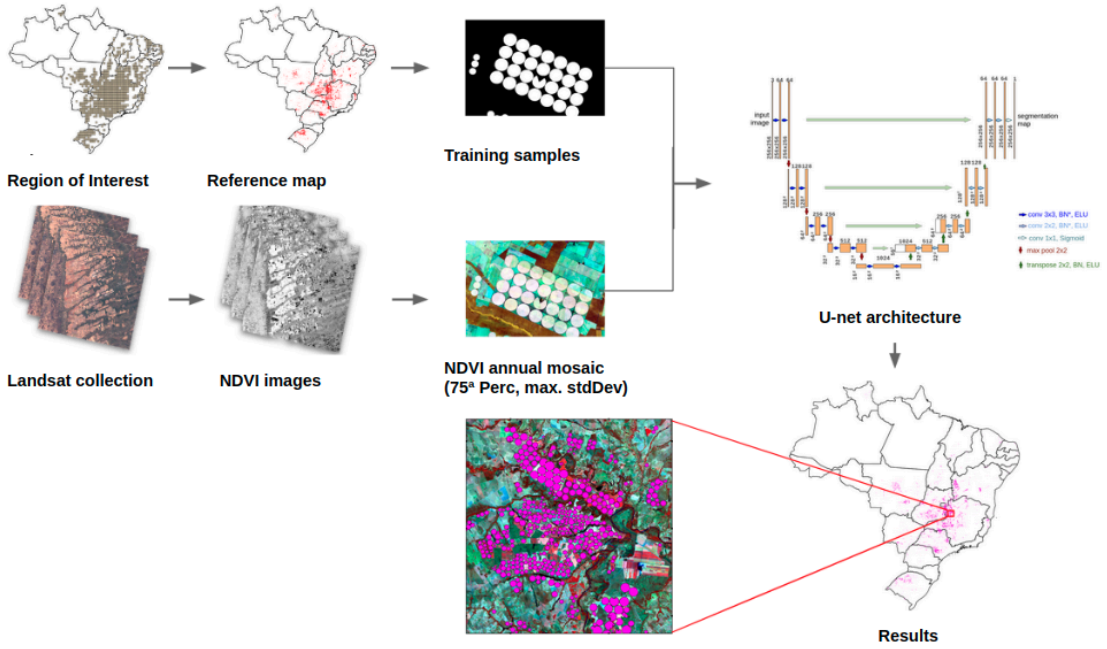


**Figure 2**: Steps of the mapping process of center pivot irrigation systems.

## 2.1 Image selection

The mapping of the center pivot irrigation systems used annual mosaics generated from available images in each year. In Collection 9, as only 2023 was added in the temporal series, the images of the period from 1985 to 2021 were Landsat Collection 1 Tier 1 TOA, and for 2022 and 2023 were Landsat Collection 2 Tier 1 TOA. In addition, only images with less than 80% cloud cover and shadows were considered.

## 2.2 Definition of regions for classification

The reference maps used for categorizing center pivot irrigation systems were generated through a collaboration between the Brazilian National Water Agency (ANA) and Embrapa Milho e Sorgo, corresponding to the years 1985, 1990, 2000, 2005, 2010, 2014, and 2017 (ANA, 2019a). These mappings were produced based on visual interpretation of imagery

acquired from Landsat 5, Landsat 8, and Sentinel 2A/2B satellites, alongside high-resolution images (<1 meter) sourced from Google Earth.

For the delimitation of the study area, the Brazilian territory was divided into blocks of 0.5 x 0.5 degrees (~300 thousand ha each). Only blocks with the occurrence of center pivot irrigation systems in any of the reference map years were selected. Figure 3 shows the 723 chosen blocks distributed across an area of approximately 212 million hectares to map center pivot irrigation systems in Brazil.

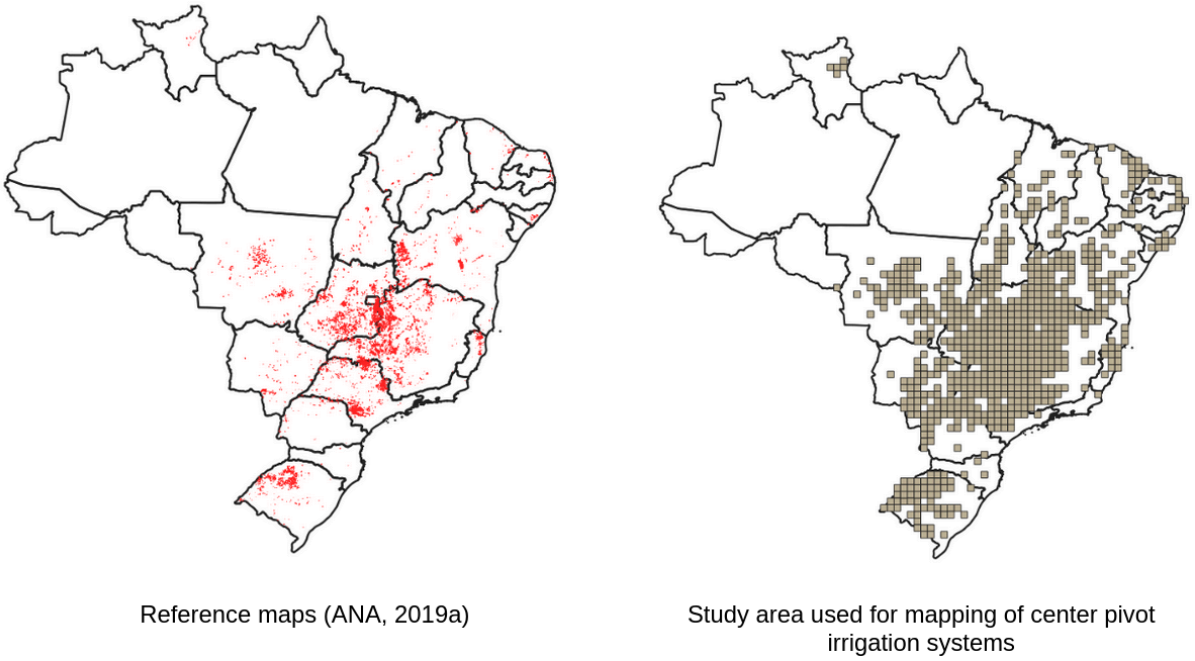


**Figure 3.** Reference maps (left) and study area (right) for the mapping of center pivot irrigation systems in Brazil.

## 2.3 Classification

### 2.3.1 Classification scheme

The classification scheme of the center pivot irrigation considered only two possible classes for each pixel, center pivot irrigation, and non-center pivot irrigation.

### 2.3.2 Feature space

The feature space created for the center pivot irrigation systems mapping aimed to obtain the characteristics of the pivot at the time they were cultivated, as well as to highlight the differences in relation to the other targets, such as other agriculture areas, pasture, forest formation, etc. Therefore, three metrics were selected that showed the best results to distinguish the pivots in relation to the other targets:

- NDVI_p75, 75th percentile of NDVI values for all images;

- NDVI_p100, 100th percentile, or maximum value, of the NDVI values of all images, and;

- NDVI_stdDev, the standard deviation of the NDVI values for all images.

The mosaic generated is composed by the selected metrics. Each metric corresponds to a band in the image, as shown in Figure 4.

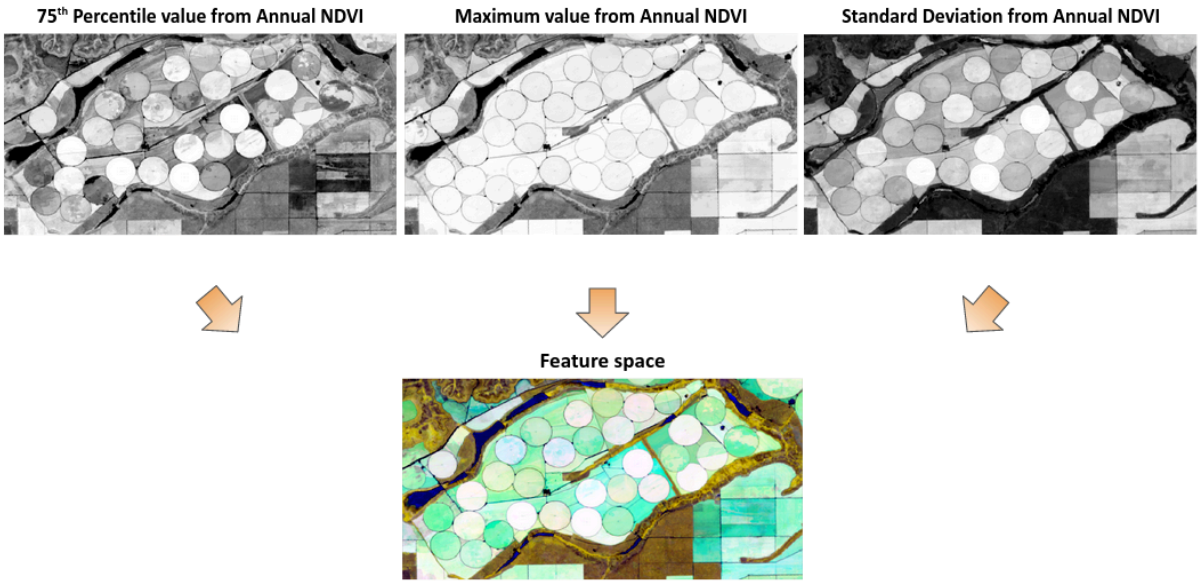


**Figure 4.** RGB visualization (NDVI p75, NDVI Maximum, NDVI stdDev) of an image used for training and mapping of the center pivot irrigation systems, generated for the year 2017.

The use of images with three bands only improved the process of training the algorithm and classifying the pivots due to the reduced computational infrastructure necessary for data processing.

### 2.3.3 Classification algorithm, training samples and parameters

Due to the extensive study area (~212 Mha) and computational limitations, the model was trained using only a subset of blocks chosen from the population of 723 blocks.

The choice of sample data is an important step for training Deep Learning models since the samples must represent all the spatial and spectral variability of the population. For this, stratified sampling was performed based on the pivot area obtained from the reference maps. The sampling considered three strata: with low, medium and high coverage of center pivot irrigation systems. The stratum containing blocks with low coverage was created from the blocks whose pivot area was less than or equal to the median of the area of all blocks, that is, 50% of the blocks (361 blocks). The stratum with the high coverage was created from blocks whose sum of the area of its pivots covers about 50% of the pivot area of the entire population (total of 41 blocks). Finally, the remaining blocks (321 blocks) were used to create the layer with blocks containing a medium cover of center pivot irrigation systems. After

creating the stratum, 20 blocks were randomly chosen for training and 10 blocks for testing in each of the three stratum. The training blocks were used to calibrate the model, while the test blocks were used later for the accuracy analysis of the model. Figure 5 illustrates the spatial distribution of the stratum and blocks chosen for training and testing the population model.

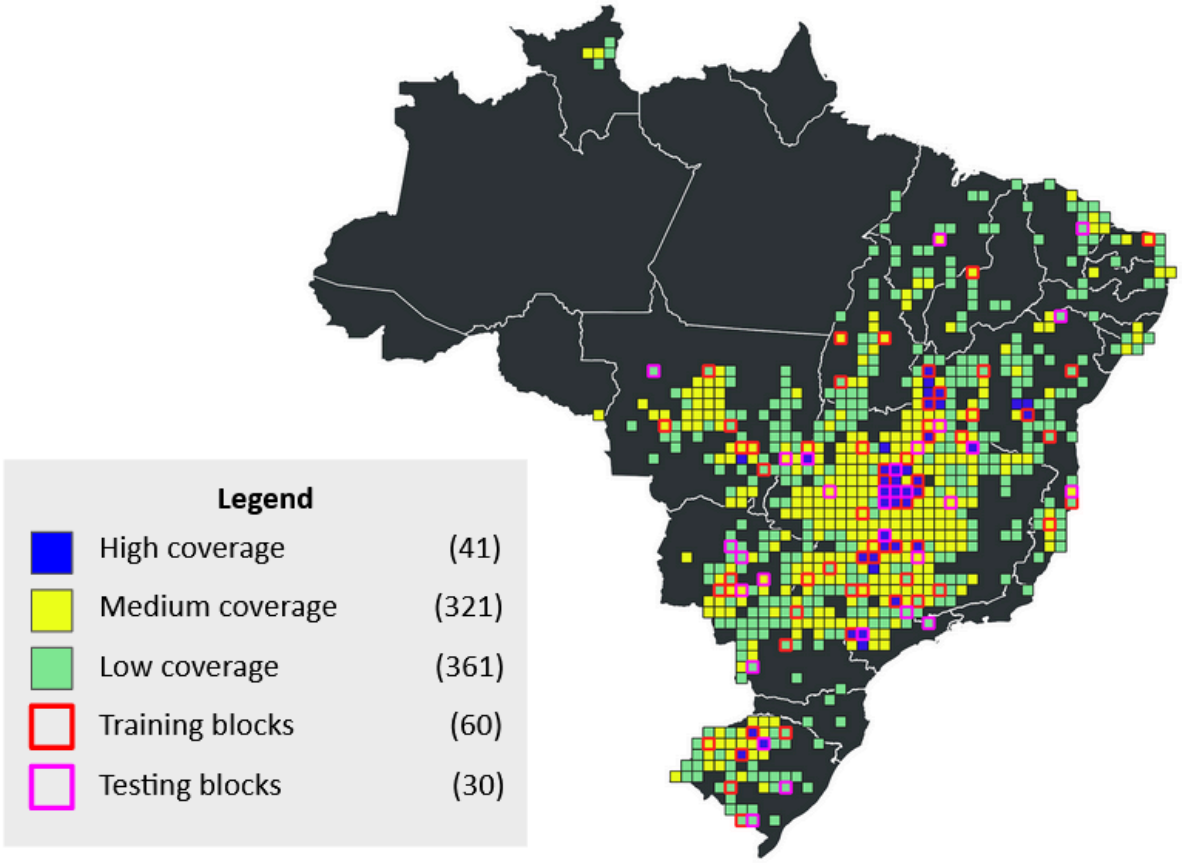


**Figure 5.** Spatial distribution of high, medium and low center pivot irrigation cover stratum and location of the blocks used for training and testing the model in Brazil.

As mentioned earlier, an adaptation of the U-Net convolutional neural network architecture was performed to map the center pivot irrigation systems. Figure 6 illustrates the modified U-Net architecture created.

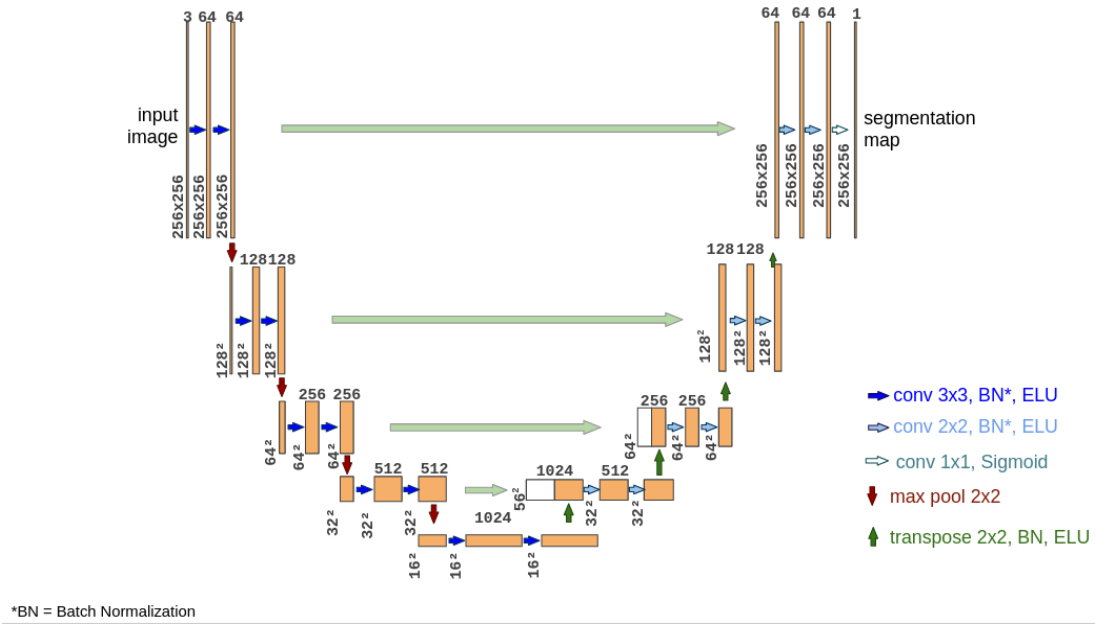


**Figure 6.** Adapted U-Net architecture, with its layers and connections, used for the mapping of center pivot irrigation systems.

This architecture was developed in Python, using the TensorFlow 2.0 library. The entire training and mapping process was carried out using the Google Colab platform using Google Drive to access the annual mosaics (generated in Google Earth Engine). Table 1 presents some hyperparameters used during model training.

**Table 1.** Hyperparameters for training the modified U-Net architecture.

| Hyperparameter | Value |
|---|---|
| Chip size | 256 x 256 pixels |
| Batch size | 20 |
| Epochs | 100 |
| Learning rate | 0.001 |

The 2017 reference map was used for model training. In the training blocks, chips with 256 x 256 pixels were generated, 75% were allocated to the training data set and 25% for the validation data set. Figure 7 illustrates the process of subdividing training blocks into smaller chips to be used as input for model training.

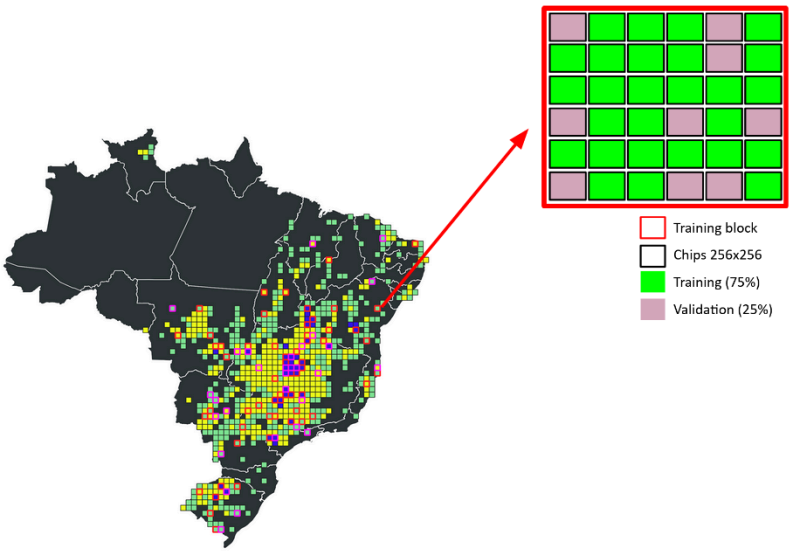


**Figure 7.** Examples of the training and validation chips allocated within the training block of the model.

The training set was used to learn the model and the validation set used to perform initial validations during model learning.

After the network training process was completed, the classifier was applied throughout the Brazilian territory. In this step, 1024 x 1024 pixel chips were used. Increasing the size of the chips at the time of sorting not only decreases problems generated by the edges of the chips but also increases the memory capacity required for processing. Therefore, it was necessary to decrease the batch size to 1.

## 2.4 Post-Classification

### 2.4.1 Temporal filter

The temporal filter employed for center pivot irrigation systems maps consisted of a five-year moving window. Within this window, the targeted pixel was modified according to two guiding rules:

1. the pixel is changed to center pivot if at least one of the two previous years and at least one of the two subsequent years, that pixel was mapped as a pivot, indicating a possible model omission error;

2. pixels that were mapped as pivots only in the assessed pixel of the five-year window, indicating a possible inclusion error, have been removed from the classification.

### 2.4.2 Spatial filter

In the center pivot irrigation systems mapping it was used a spatial filter based on the erosion operation followed by an expansion operation using a circular kernel with a radius of

60 meters. This spatial filter helped to eliminate noise generated by the mapping, as well as smoothing the edges of the center pivot irrigation (Figure 8).

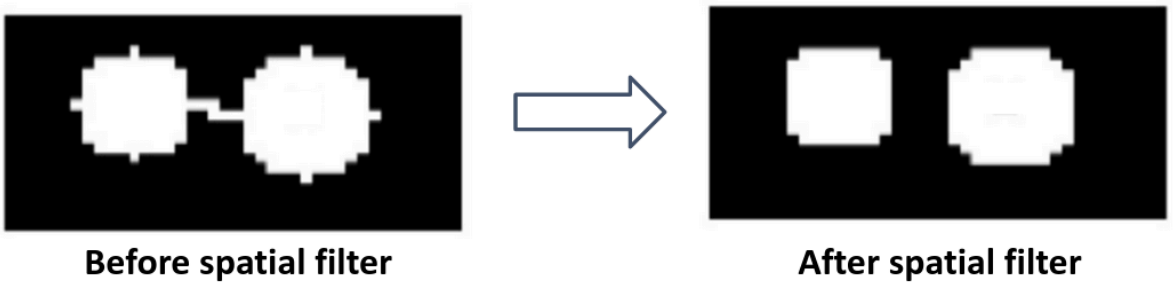


**Figure 8** Example of correction of the spatial filter (on the right) in a classification that presents noise on the edges (on the left).

### 2.5 Validation strategies

The preliminary validation of the center pivot irrigation model used the test blocks of the 2017 mapping (see Figure 5), as these blocks were not used for the model training. From the reference map, the user's and producer's accuracy was calculated for each of the individual stratum and also considering all strata at the same time. Table 2 presents the results of the preliminary model validation.

**Table 2.** Preliminary validation of the center pivot irrigation mapping for the year 2017, using the test blocks selected in each stratum.

| Stratum | Producer's Accuracy | User's Accuracy |
|---|---|---|
| Low coverage | 40.87% | 71.39% |
| Medium coverage | 86.37% | 91.62% |
| High coverage | 84.16% | 96.19% |
| All strata | 83.97% | 95.38% |

The preliminary accuracy analysis showed that, in 2017, the model performed better in regions with higher center pivot coverage. Considering all strata in 2017, the model presented an omission error of 16% and an inclusion error of 5%.

## 2.6 Results

Comparing the area mapping results between MapBiomas Collection 9 and the ANA/EMBRAPA dataset reveals that until 2020, the area mapped by MapBiomas closely aligns with the values reported in the ANA/EMBRAPA dataset. However, in the subsequent years, emerges a more substantial discrepancy, with MapBiomas Collection 9 showing a tendency to underestimate the actual area.

Over the temporal series, the ANA/EMBRAPA dataset indicates an initial area of approximately 0.03 Mha in 1985. This area steadily increases, reaching its peak of 1.90 Mha in 2020. In comparison, MapBiomas Collection 9 starts at about 0.1 Mha in 1985, and its growth remains consistent, culminating at around 1.65 Mha in 2022 (Figure 9).

In addition, is important to point out, that these divergences between the MapBiomas and ANA/EMBRAPA, especially in the last years, underscores the significance of comprehending their distinct methodologies and sources, mainly due to the omission of the smalls pivots from MapBiomas.

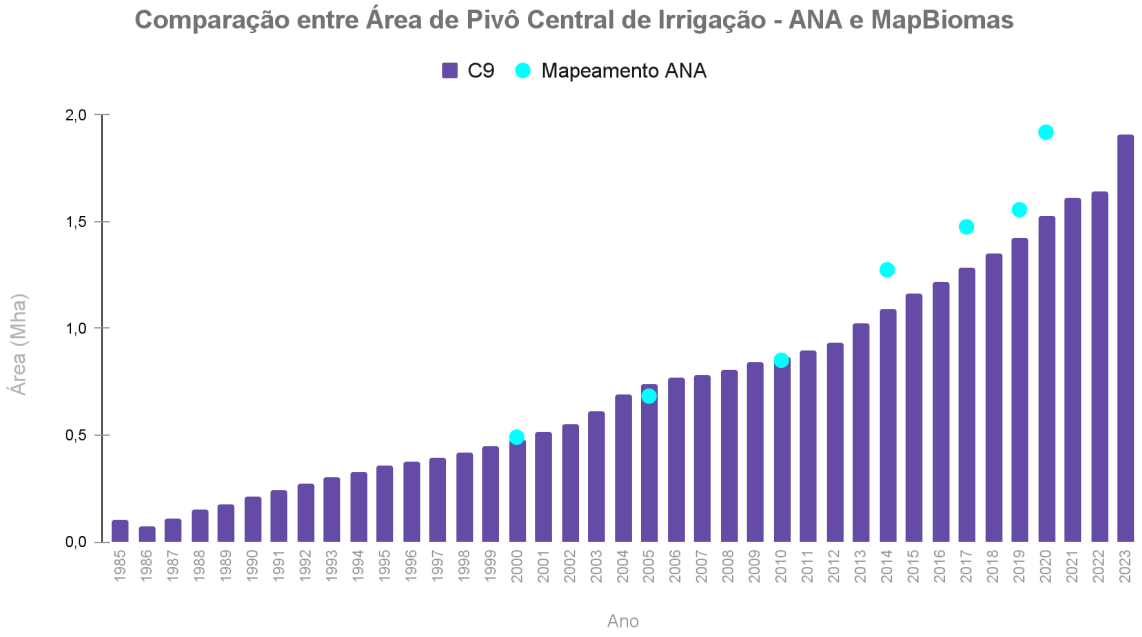


**Figure 9:** Results of automatic mapping of center pivot irrigation systems in Brazil based on Landsat images for the period from 1985 to 2023 compared to surveys carried out by the ANA (ANA, 2022).

## 3 Irrigated rice

An improvement in the mapping rice to collection 9 was the inclusion of Random Forest algorithm, to complement the result obtained with U-net U-Net architecture, a segmentation convolutional neural network architecture (RONNEBERGER et al., 2015). As in previous collections, the methodology for mapping 'Irrigated rice' is also based on Landsat imagery.

The adapted U-Net architecture is trained with irrigated rice samples obtained by reference maps from National Water Agency (ANA, 2021b) and the National Supply Company (Conab, 2020). To increase the temporal and spatial consistency of the final maps, the raw result is also post-processed using temporal and spatial filters. Figure 10 presents a flowchart of the methodology for irrigated rice classification.

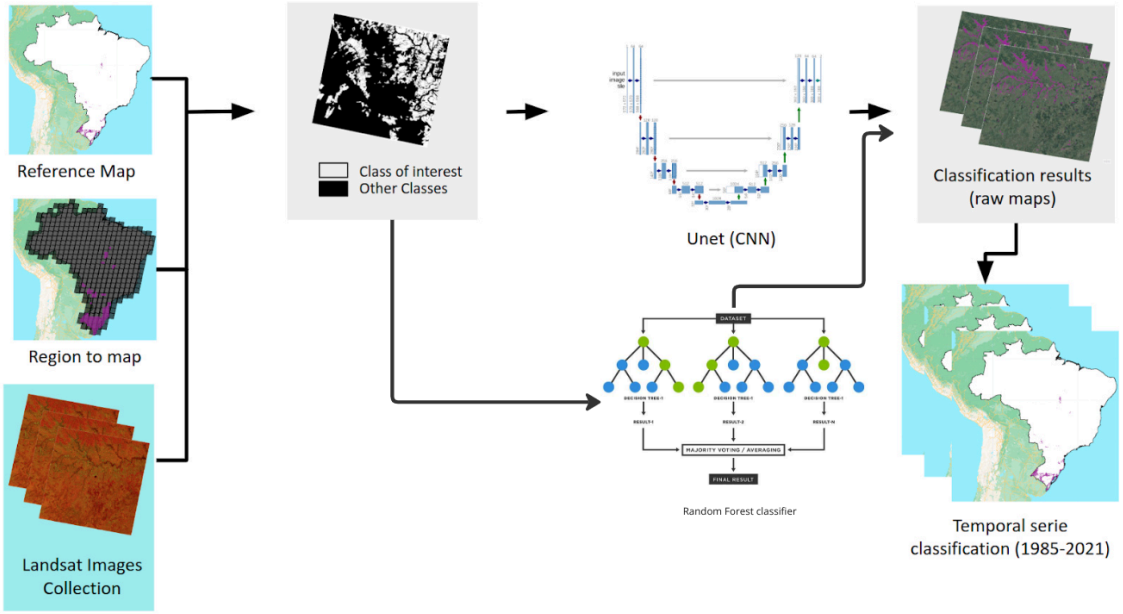


**Figure 10.** Classification process for mapping irrigation rice in MapBiomas Collection 9.

### 3.1 Image selection

Due to variations in agricultural practices, cropping systems, soil management, and vegetation patterns, compounded by computational limitations that restrict the utilization of diverse images and their associated attributes, distinct models were developed using specific mosaics built to each geographical region. This approach aimed to enhance the visibility of rice plots within these mosaics, thereby facilitating the training of the models. Consequently, three distinct mosaic types were generated to train separate models, with each model designed for a specific Brazilian state.

To construct these mosaics, we initially sourced TOA images from collections of TM sensors (spanning from January 2000 to October 2011), ETM+ (ranging from January 2000 to May 2003 and October 2011 to March 2013), and OLI (covering March 2013 to December 2019). Subsequently, images capturing both the growing and off-seasons of irrigated rice were selected, the choice of which depended on the particular region being considered.

A critical subsequent step involved the meticulous removal of cloud cover and cloud shadows from the images. This process was achieved by leveraging the data encapsulated within the Landsat quality band metadata (QA band). The images chosen for inclusion were contingent on aligning with the growing and off-season periods as delineated by the annual mapping schedule of each state, as detailed in Table 3.

**Table 3**. Periods used for the selection of images that were used to compose the mosaics used for the mapping of irrigated rice in Collection 9.

| State | Start season | End season | Start off-season | End off-season |
|---|---|---|---|---|
| Tocantins - TO | 04/01/year | 07/30/year | 08/01/year-1 | 11/01/year-1 |
| Rio Grande do Sul - RS | 10/01/year-1 | 04/01/year | 01/10/year-1 | 01/01/year |
| Santa Catarina - SC<br>Paraná - PR | 10/01/year-1 | 04/30/year | 01/01/year | 07/30/year |

### 3.2 Definition of regions for classification

The delimitation of the mapping area was based on the map of irrigated rice in Brazil published by the National Water Agency (ANA, 2021b) and the National Supply Company (Conab, 2020) and a map produced by Remap, specifically on Marajó Island, state of Pará. The selection of images was made based on the season period according to the year of mapping carried out in each state. The reference map was divided into blocks of 0.5 x 0.5 degrees (~300 thousand ha each). The blocks used for irrigated rice mapping and training were those that overlapped the reference map and with the states of interest, as illustrated in Figure 11.

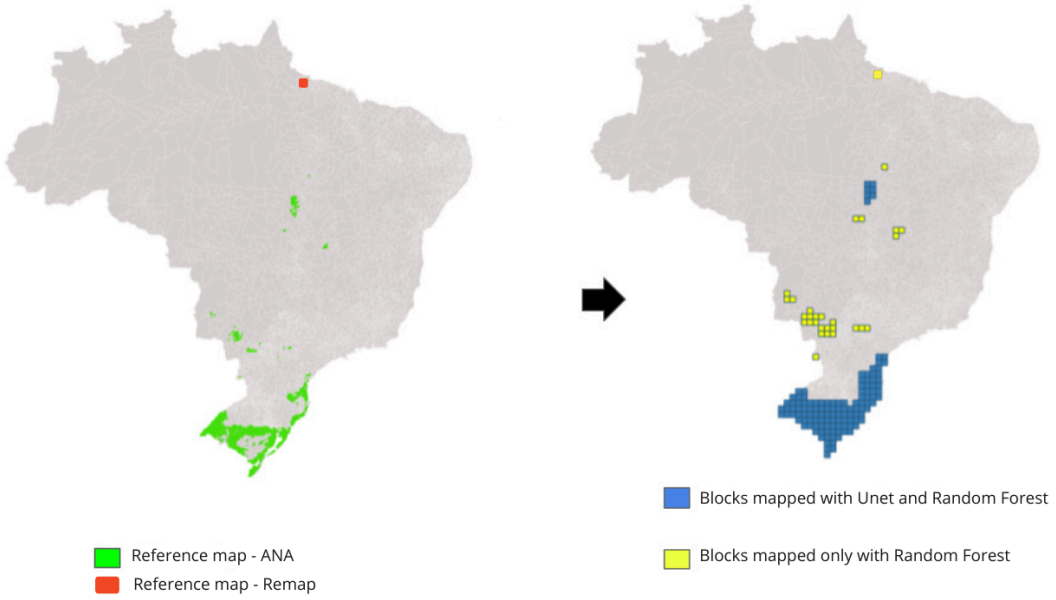


**Figure 11.** Study area used for the mapping of irrigated rice in the MapBiomas Project.

### 3.3 Classification

#### 3.3.1 Classification scheme

Each of the three Brazilian states chosen was mapped by a model specifically trained for that region. The classification considered two classes (binary classification), 1 for 'Irrigated rice' and 0 for 'non-Irrigated rice'. Both algorithms used the same approach.

#### 3.3.2 Feature Space

The feature space for mapping irrigated rice using the adapted U-Net architecture and Random Forest classifier was designed to accentuate the most significant distinctions between Irrigated rice crops and other land uses, such as other agricultural crops. The choice of variables within this feature space was contingent upon the specific Brazilian state undergoing mapping, as presented in Table 4.

| State | Tocantins - TO | Rio Grande do Sul - RS | Santa Catarina - SC Paraná - PR | Goiás - GO | Pará - PA | Mato Grosso do Sul - MS |
|---|---|---|---|---|---|---|
| **Bands** | SWIR1, SWIR2 | SWIR1, SWIR2, TIR1 | SWIR2 | SWIR1, SWIR2 | SWIR1, SWIR2 | SWIR2 |
| **Indexes** | EVI2, NDWI | EVI2 | EVI2, NDWI | EVI2, NDWI | EVI2, NDWI | EVI2, NDWI |
| **Metrics** | CEI (EVI2), CEI (NDWI) | CEI (EVI2) | CEI (EVI2), CEI (NDWI) | CEI (EVI2), CEI (NDWI) | CEI (EVI2), CEI (NDWI) | CEI (EVI2), CEI (NDWI) |
| **Period** | Bands - off season CEI - Annual | Bands - season CEI - Annual | Bands - off season CEI - Annual | Bands - off season CEI - Annual | Bands - off season CEI - Annual | Bands - off season CEI - Annual |

**Table 4:** Bands, indexes, and metrics used to compose the Landsat mosaics to classify Irrigated rice.

Figure 12 illustrates the different image mosaics that were used to map irrigated rice in the evaluated Brazilian states.

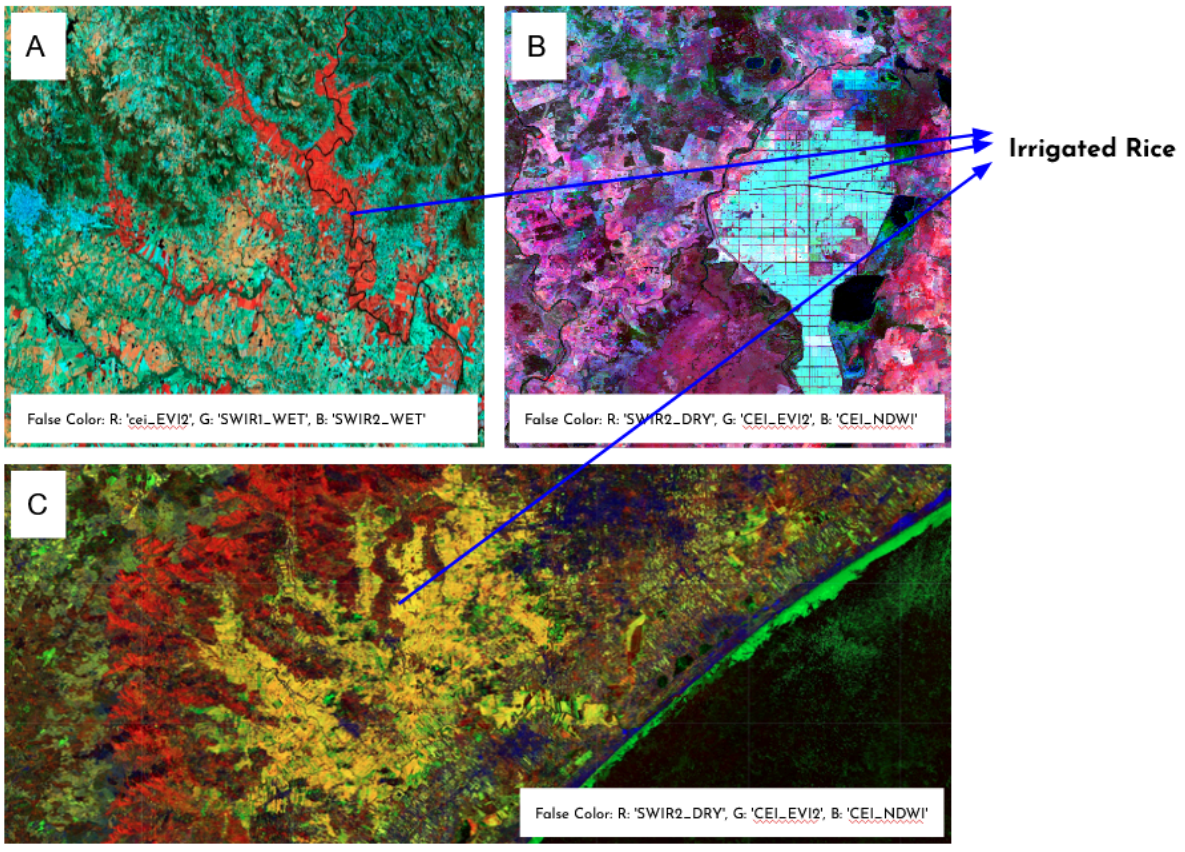


**Figure 12.** RGB visualization of the mosaics used for the mapping of irrigated rice in the states of Rio Grande do Sul (A), Tocantins (B) and Santa Catarina (C).

### 3.4 Classification algorithm, training samples and parameters

For the U-Net model, to obtain the training, validation and test sets, each of the training blocks was first traversed with a moving window, generating chips with 256 x 256 pixels. Then, for each block, the generated chips were divided into 70, 20 and 10% for training, validation and test sets, respectively. The training and validation datasets were used in the model adjustment and pre-validation processing during model training, while the test dataset was used only for final validation of the already trained model.

After the separate data sets, the pixel values of each feature were normalized. The normalization rescaled the numerical values of the features to the range 0 to 1, making each feature contribute similarly to the calculation of model loss. In Figure 13, an example of the mosaic and its respective reference map is shown.

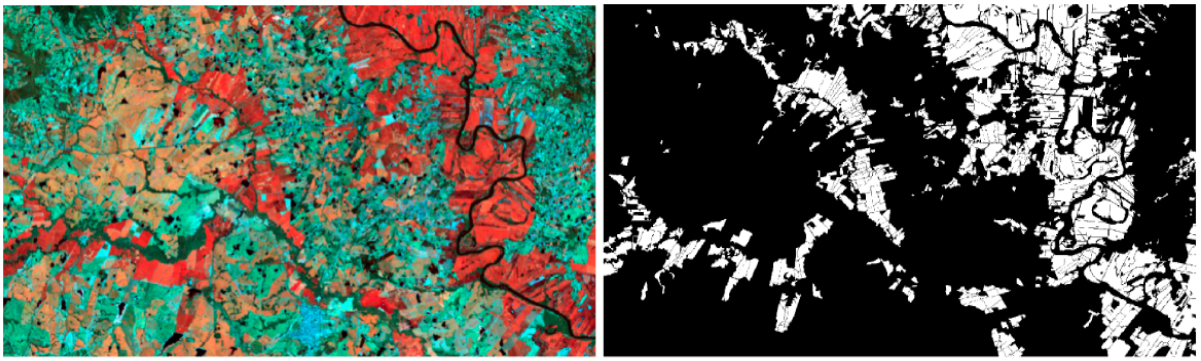

**Figure 13.** Example of an image mosaic used to train one of the models and its respective ground truth containing classes 1 (Irrigated rice) and 0 (non-Irrigated rice).

### 3.5 Post-Classification

In the post-processing step of irrigated rice mapping, an noise filter was not used, since the U-Net algorithm demonstrates reduced vulnerability to isolated noise instances compared to pixel-by-pixel algorithms like Random Forest. Additionally, temporal filters were also not applied to the irrigated rice mapping, due the consideration of the distinctive planting dynamics of rice, particularly within the Pampa biome, which constitutes the largest rice-producing region in Brazil. In this biome, rice cultivation areas are intertwined with rotational practices involving cattle and fallow periods. Consequently, the intricate and variable nature of these dynamics precludes the practical implementation of temporal filters without disregarding these dynamics.

### 3.6 Validation strategies

For the result obtained by U-Net, an analysis of the model's accuracy was carried out on the chips that were allocated in the dataset of the test. The metric adopted for the initial validation was the Dice Coefficient. The Dice Coefficient represents **2 * the Area of Overlap divided by the total number of pixels in both images** with values ranging from 0 to 1, with 1

signifying the greatest similarity between predicted and truth. Table 5 presents the results of Dice Coefficient for each region considered for the Irrigated rice mapping.

**Table 5.** Metrics used to classify irrigated rice in MapBiomas Collection 9.

| Region | Evaluated chips | Dice Coefficient |
|---|---|---|
| Rio Grande do Sul - RS | 536 | 0.69 |
| Santa Catarina - SC | 140 | 0.44 |
| Tocantins - TO | 288 | 0.40 |

The result of the model evaluation and the visual analysis of the mapping indicate that the model had a better performance in the state of Rio Grande do Sul, a region with most of the irrigated rice area. Regarding the detailing of the mapping, the model had greater difficulty in delimiting the borders of the agricultural plots, which may partially justify the values of the Dice Coefficient.

### 3.7 Results

The area resulting from the automatic mapping of irrigated rice from Collection 9 was compared with the area of total and irrigated rice, adapted from the "Levantamento Sistemático da Produção Agrícola - IBGE 1986-2020" (EMBRAPA, 2020) (Figure 14).

When comparing the values of irrigated rice area between MapBiomas and the EMBRAPA dataset, certain trends have become evident over the years. This comparison highlights how the two datasets portray diverse patterns in reporting irrigated rice areas, possibly due to distinct data sources and methodologies.

The EMBRAPA dataset demonstrates a gradual increase in irrigated rice area, starting with 1.10 Mha in 1985 and reaching approximately 1.30 Mha in 2022. In contrast, MapBiomas Collection 9 exhibits an initial area of 0.45 Mha in 1985, followed by 0.48 Mha in 1986. It then showcases an oscillatory trend before peaking at 1.38 Mha in 2022, with the most recent mapped area in 2023 being 1.02 Mha.

While both datasets illustrate an overall upward trend, the differences in reported values stem from the complexities of data collection, processing, and methodology. Particularly significant is the observable variation in the datasets' estimates over the years, underscoring the importance of methodically evaluating their respective methodologies and sources. This practice is essential to derive accurate insights concerning irrigated rice cultivation trends in the mapping regions.

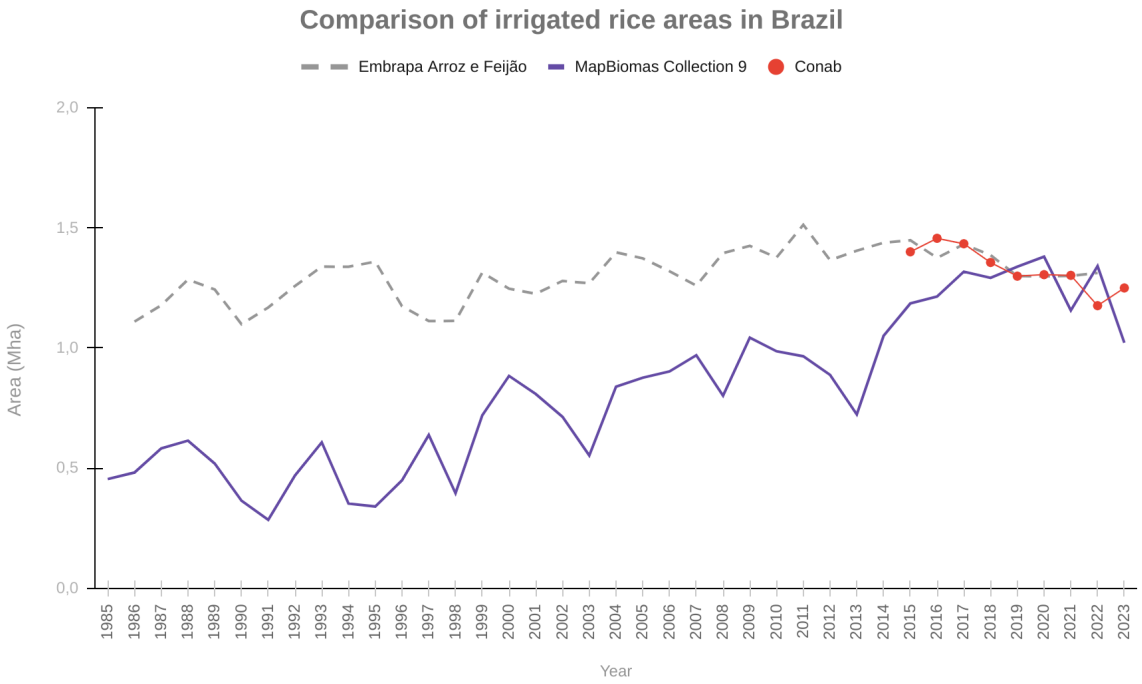


**Figure 14**. Comparison between rice areas obtained from the MapBiomas Collection 9 and data provided by the Embrapa Arroz e Feijão (1986-2022) and Conab.

## 4 Irrigated agriculture in the semi-arid region

In Collection 9, a notable improvement in the approach employed for classifying the 'Other irrigation systems' class is worth mentioning. The methodology maintains its foundation in pixel-by-pixel mapping through the utilization of the Random Forest algorithm. However, in the Collection 9, a novel reference map of irrigated agriculture in the semiarid region was acquired in collaboration with the National Water Agency (ANA). Additionally, a regular grid was obtained from ANA, demarcating regions within the semiarid region where occurrences of irrigated crops are prevalent. These improvements to the methodology serve to enhance the accuracy and precision of the mapping process for the 'Other irrigation systems' class. Figure 15 presents the flowchart of the methodology for 'Other irrigation systems' classification

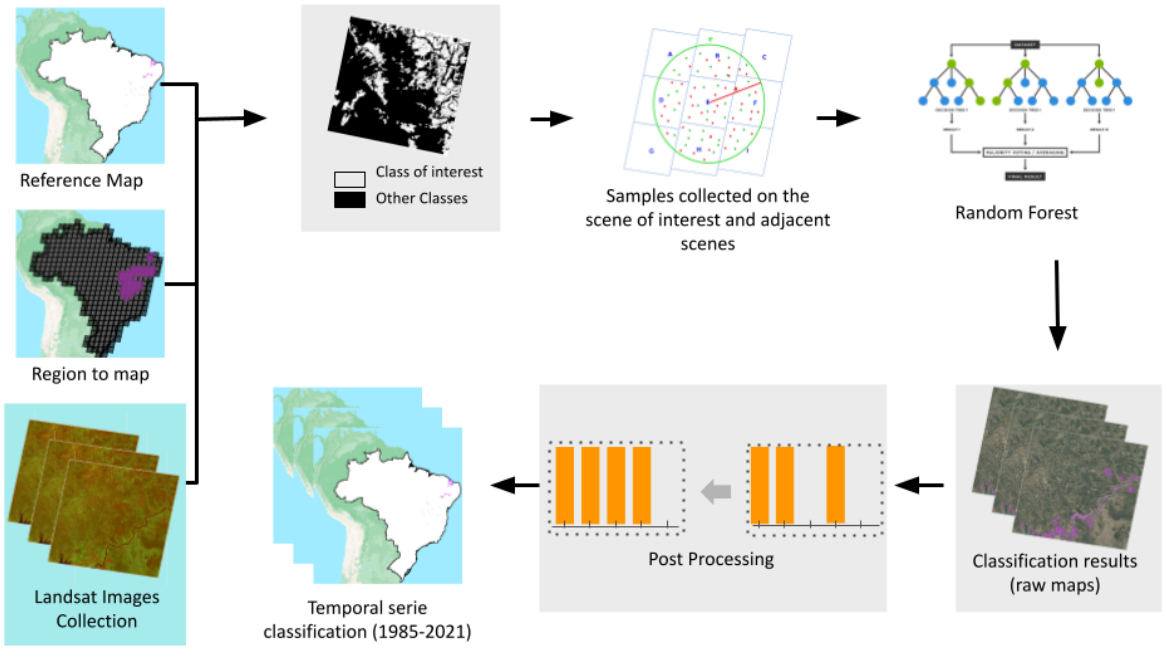


**Figure 15.** Classification process for mapping 'Other irrigation systems' in MapBiomas.

### 4.1 Image selection

In this new approach for Collection 9, the mapping process relied on the use of yearly TOA (Top of Atmosphere) mosaics from Landsat Collection 2. These mosaics were supplemented by a set of spectral indices and statistical measures. This combination aimed to emphasize and distinguish between areas of irrigated agriculture and the native vegetation. By incorporating these spectral indices and statistical measures, the methodology gains the ability to identify and highlight the distinct features that characterize irrigated agricultural areas within the context of the surrounding natural vegetation.

### 4.2 Definition of regions for classification

In the mapping of other irrigation systems, the study area was restricted to the Brazilian semi-arid region. Due to water limitations, irrigation is almost a mandatory requirement in this region to reduce production risks and/or increase productivity.

In the previous Collections, a total of 34 municipalities comprised the mapping area (selected due to their substantial expanse of irrigated agriculture). However, several of these municipalities also hosted significant non-irrigated agricultural activity, inadvertently leading to the inclusion of non-irrigated areas being classified as irrigated in the resulting map. The mapping accuracy was compromised due to the overlap with non-irrigated regions.

With the adoption of the new approach in Collection 9, a substantial enhancement in mapping accuracy has been achieved. This enhancement is attributed to the utilization of a regular grid provided by the ANA covering the semi-arid regions with irrigated agriculture. Each grid cell measures approximately 0.20° x 0.20° in size. This new grid-based approach

has helped to avoid the previous issue of misclassification of non-irrigated areas. Figure 16 presents a comparison between the region adopted in the previous Collections and the new grid-based region adopted in Collection 9 to map the 'Other Irrigation System' class. This transition to the grid-based methodology has resulted in improved accuracy and a more precise representation of irrigated areas.

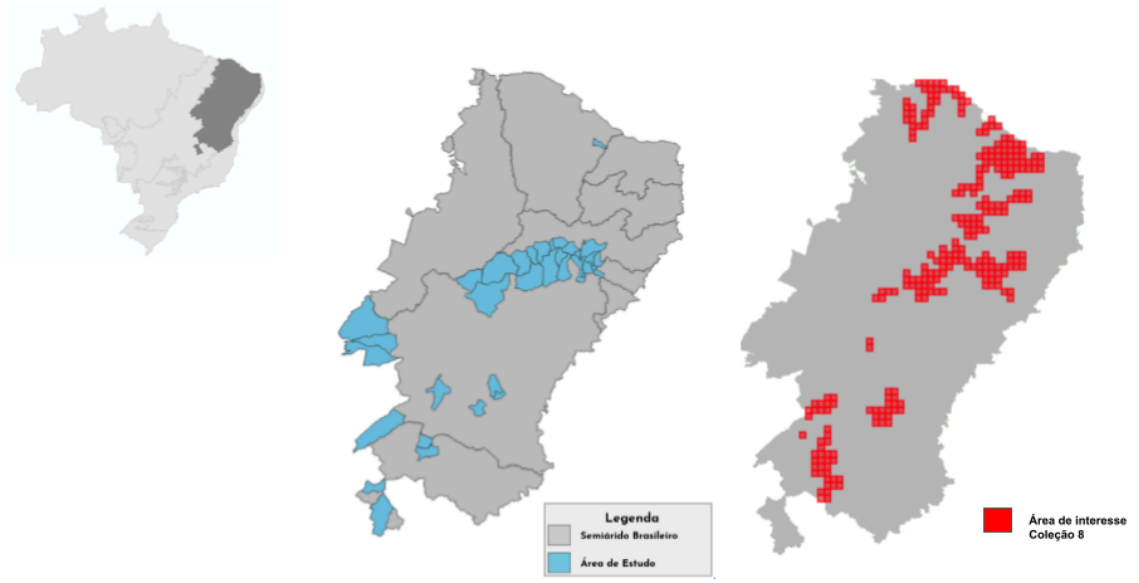


**Figure 16.** Comparison between the region adopted in the previous Collections and a new region adopted since Collection 8 to map ‘Other Irrigation System’ class.

## 4.3 Classification

### 4.3.1 Classification scheme

The classification process for the 'Other irrigation systems' class involves the consideration of two main groups: 'Irrigated agriculture' and 'Non-irrigated agriculture'. To enable the mapping of this class, training samples are obtained from the reference map provided by the ANA. These training samples cover both 'Irrigated agriculture' and 'Non-irrigated agriculture' regions and are used as training for the Random Forest classifier. This trained classifier is subsequently used to identify areas of irrigated agriculture within the annual Landsat mosaics. This classification procedure is carried out exclusively within the geographical boundaries set by the ANA's GRID, ensuring accuracy in identifying irrigated agricultural regions.

### 4.3.2 Feature space

For the mapping of 'Other irrigation systems' alongside the data obtained from Landsat program satellites, supplementary metrics and indices were also calculated to enhance the identification of irrigated agricultural areas.

Table 6 presents the set of annual metrics used to map irrigated agriculture in the Brazilian semi-arid region.

**Table 6.** Set of metrics used to map irrigated agriculture in the Brazilian semi-arid region.

| Source | Bands and Spectral indices | Metrics |
|---|---|---|
| Landsat | BLUE | EVI2 Quality Mosaic |
| | GREEN | Minimum |
| | RED | Maximum |
| | NIR | Median |
| | SWIR1 | Standard Deviation |
| | SWIR2 | |
| | TIR1 | |
| | EVI2 (JIANG et al, 2008) | |
| | NDWI (GAO, 1996) | |
| | MNDWI (XU, 2006) | |
| | CAI (NAGLER et al, 2003) | |

### 4.4 Classification algorithm, training samples and parameters

The methodology employed for mapping irrigated agriculture within the semiarid region was founded on the application of the Random Forest algorithm. It used annual Landsat image mosaics, incorporating Landsat spectral bands—specifically, BLUE, GREEN, RED, NIR, SWIR1, SWIR2, and TIR1. These spectral bands yielded valuable insights into both physical and biological surface attributes, facilitating the accurate differentiation of distinct land cover classes. Furthermore, statistical metrics such as Minimum, Maximum, Median, and Standard Deviation were computed for each spectral band, along with the EVI2 Quality Mosaic. This augmentation aimed to refine the spectral signal of the target class. Additionally, a selection of vegetation indices, EVI2, NDWI, CAI, and MNDWI, were integrated into the analysis to further enhance the classification process.

To initiate the process, 10,000 training samples were collected for both the 'Irrigated

agriculture' and 'Non-irrigated agriculture' classes, considering the reference map provided by the ANA for the year 2019. These training samples were strategically acquired within the designated grids of the irrigated agriculture region in the semiarid region, as outlined by the ANA.

The Random Forest model was trained using these training samples and the Landsat mosaics, with a total of 100 trees in the model. The classification procedure was exclusively confined to grids demarcated by the ANA, aligning with their predefined geographical boundaries. The assimilated training samples corresponded to the ANA's reference map, guaranteeing the accurate representation of 'Irrigated agriculture' and 'Non-irrigated agriculture' across the region.

### 4.5 Post-Classification

The post-classification process of irrigation agriculture maps included the application of temporal and spatial filters.

#### 4.5.1 Temporal filter

In the other irrigation systems mapping, a moving five-year window was also used, but using a different rule from the center pivot irrigation systems. In this filter, if the evaluated pixel was in the same class as at least three other pixels (previous, ahead or both), it remains in that class. However, if the evaluated pixel was not of the same class as at least three pixels (previous, ahead or both), the class was changed.

#### 4.5.2 Spatial filter

In the other irrigation systems, a spatial filter was used to remove pixels that had less than 6 other connected pixels.

## 4.6 Results

When evaluating the 'Other irrigation systems' class mapped by MapBiomas Collection 9 and comparing it with ANA and IBGE data, discernible trends and disparities become evident (Figure 17). This examination underscores the variability in reported values among the datasets, which may arise from differing data sources, methodologies, and assessment scopes.

In contrast, ANA data provides information for specific years, indicating an area of 0.34 Mha in 2015 and 0.32 Mha in 2019. Similarly, IBGE data, available for 2017, records an area of 0.26 Mha for the 'Other irrigation systems'.

While the datasets exhibit overall upward trends, the variations between reported values reflect differences in data collection, processing, and methodologies. It is noteworthy that the ANA and IBGE data, are collected at specific intervals, whereas MapBiomas Collection 9 provides a continuous temporal perspective. These disparities emphasize the importance of evaluation and cautious interpretation when utilizing such datasets to comprehend land use dynamics and trends of 'Other irrigation systems' class.

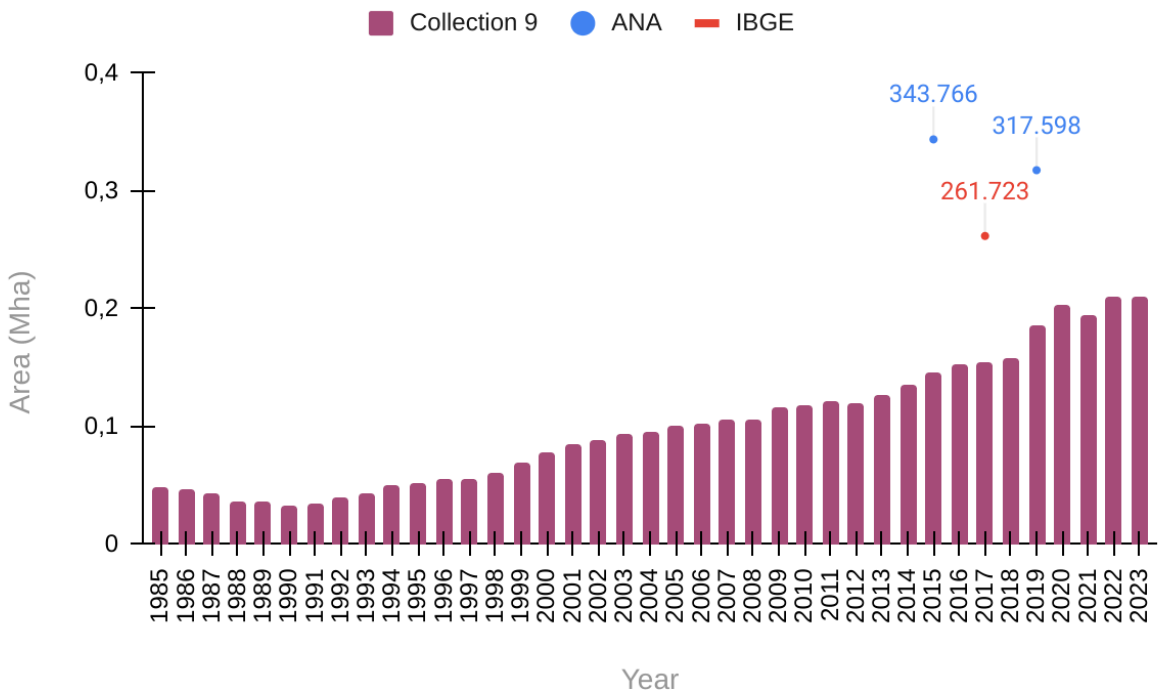


**Figure 17.** Results of the 'Other irrigation systems' class in the semiarid region for the period from 1985 to 2022 compared to surveys carried out by the *Atlas da Irrigação* (ANA, 2017, 2021a) and the *Censo Agropecuário* (IBGE, 2009, 2019).

**Center pivot irrigation information (*Beta*)**

Understanding center pivots irrigation dynamics allows us to improve our understanding about most parts of irrigated agriculture in Brazil. The first effort to understand irrigation systems in the MapBiomas project began in Collection 5, with the use of innovative methods of Artificial Intelligence, through convolutional artificial neural networks to perform semantic segmentation of pivots throughout the Brazilian territory. In Collection 6 there was an expansion of the years mapped, with generation of time span maps of the entire MapBiomas series. In Collection 7.1 in addition to another time series expansion of center pivot irrigation map, covering from 1985 until 2021, it was also made an effort to improve our understanding about crop dynamics in center pivot irrigation. Then, in Collection 7.1, a methodology was developed to provide more detailed information about this system, such as the number of cycles performed per pivot in the crop year, the dates of start and end of each cycle, in addition to information about accumulated precipitation in each pivot and each crop cycle, initially only for Minas Gerais state between 2015 and 2021. In Collection 8 and 9, the pivot dynamic was extented to the entire Brazilian territory, and the 2022 and 2023 years, respectively, were also processed, providing dynamic information about the pivots from 2015 to 2023.

### 4.7 Overview of the classification method

To provide this information on each pivot, several steps are necessary, from applying a Deep Learning model for center pivot irrigation individualization to obtaining smoothed time curves to identify the number of annual cycles existing in each of these pivots. Figure 18 presents all the steps of this methodology.

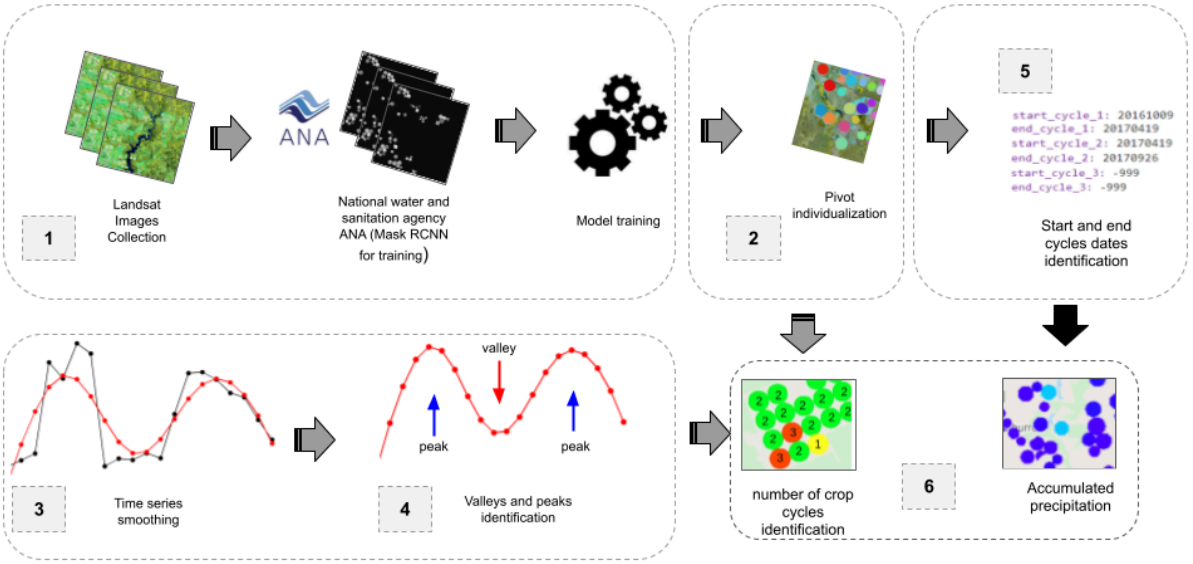


**Figure 18.** Flowchart of the methodology necessary to obtain the number of cycles per pivot. 1) Obtaining the training dataset for the neural network (Landsat image and Mask of pivots);

2) Training the Deep Learning model for individualization of the pivots; 3) Landsat time series curve smoothing; 4) Identification of peaks and valleys in the curve; 5) Identification of the start and end dates of each cycle; and 6) Obtaining number of crop cycles and accumulated precipitation per cycle per pivot.

## 4.8 Center pivot individualization

### 4.8.1 Image selection

To individualize each center pivot irrigation, we used annual mosaics generated from available images for each year. Therefore, images from the Landsat series were obtained on the Google Earth Engine platform (Collection 2 Tier 1 TOA) in the period of 2015 to 2023. Only images with under 80% cloud cover and shadows were considered.

### 4.8.2 Definition of regions for classification

To individualize each center pivot irrigation, samples were first selected that represent relevant information about the pivots, so it was decided to select the blocks that contained at least 5 pivots. Thus, the samples were stratified between test areas (blocks with at least 5 and at most 9 pivots) and training areas (blocks with more than 10 pivots).

Figure 19 presents the blocks used for the RCNN (Region Based Convolutional Neural Networks) Mask prediction for all Brazil. The Mask R-CNN is a Convolutional Neural Network (CNN) and state-of-the-art in terms of image segmentation. This variant of a Deep Neural Network detects objects in an image and generates a high-quality segmentation mask for each instance.

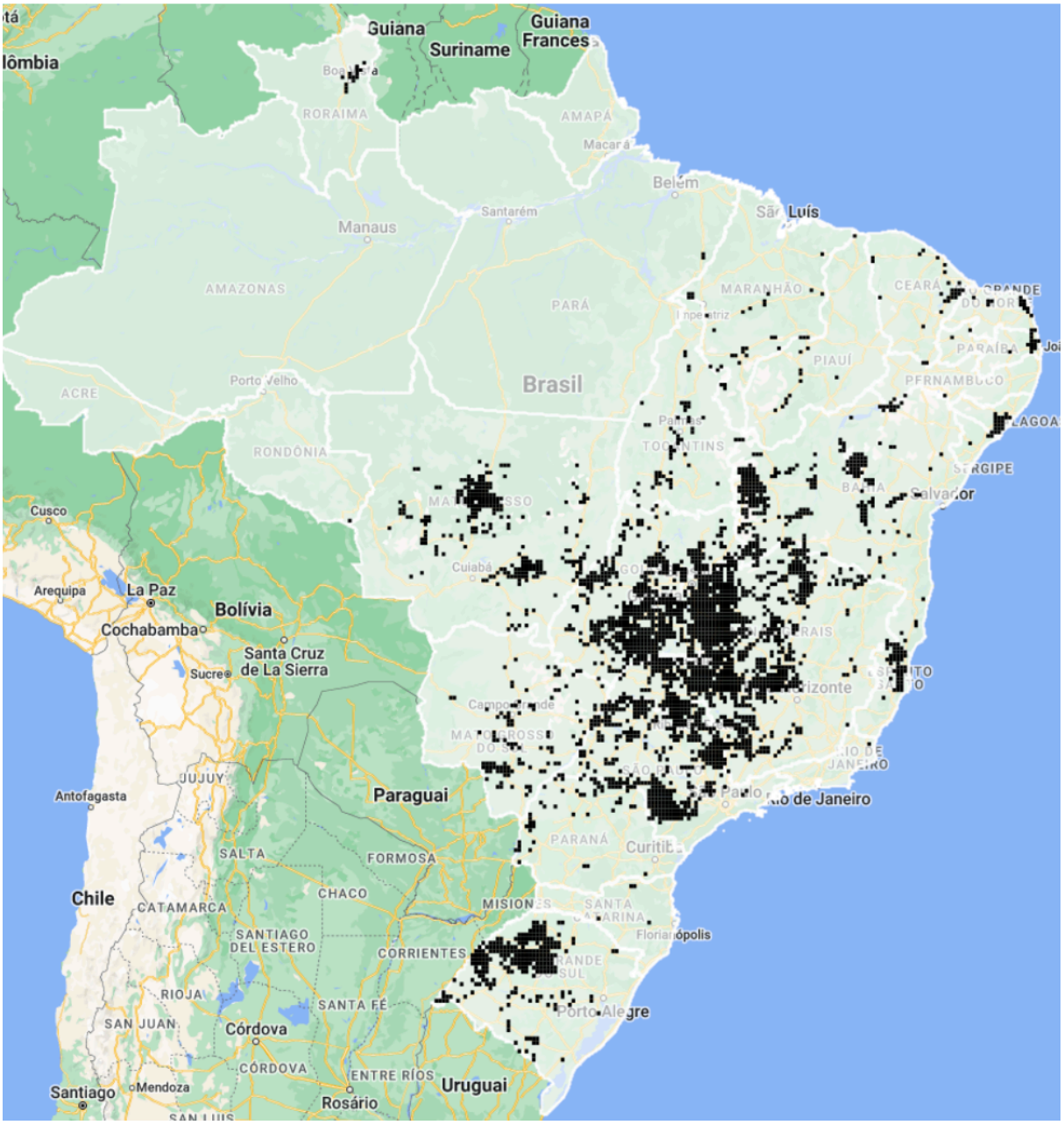


**Figure 19.** A) Tiles (grid in black) for RCNN Mask prediction. Note: Areas without tiles indicate the non-existence of irrigation center pivots, according to the map made available by ANA for the year 2019.

### 4.8.3 Classification

#### 4.8.3.1 Classification scheme

The RCNN was trained to identify and individualize each center pivot irrigation. Semantic segmentation considers two classes, (binary classification), 1 for 'pivot' and 0 for 'non pivot'. In instance segmentation, however, each pivot is mapped separately, adding a unique ID for each.

#### 4.8.3.2 Feature space

The Normalized Difference Vegetation Index (NDVI) (ROUSE et al., 1974) was calculated for each image in order to generate standard deviation and percentiles metrics, as presented in Table 8. These metrics were chosen seeking to capture not only the temporal variation of NDVI in the pivots, but also the variations of other agricultural targets outside of pivots (such as pasture, barren soil, native vegetation, etc).

**Table 8.** Index and metrics used to individualize center pivot irrigation.

| | |
|---|---|
| **Indexes** | NDVI |
| **Metrics** | stdDev, 75th percentile, 100th percentile |

#### 4.8.3.3 Classification algorithm, training samples and parameters

Instance segmentation is performed from a pre-trained neural network of Mask RCNN type architecture. This architecture was developed in Python, using the Pytorch framework, along with the Detectron 2 package. Figure 20 represents the flowchart of the entire Mask RCNN training process.

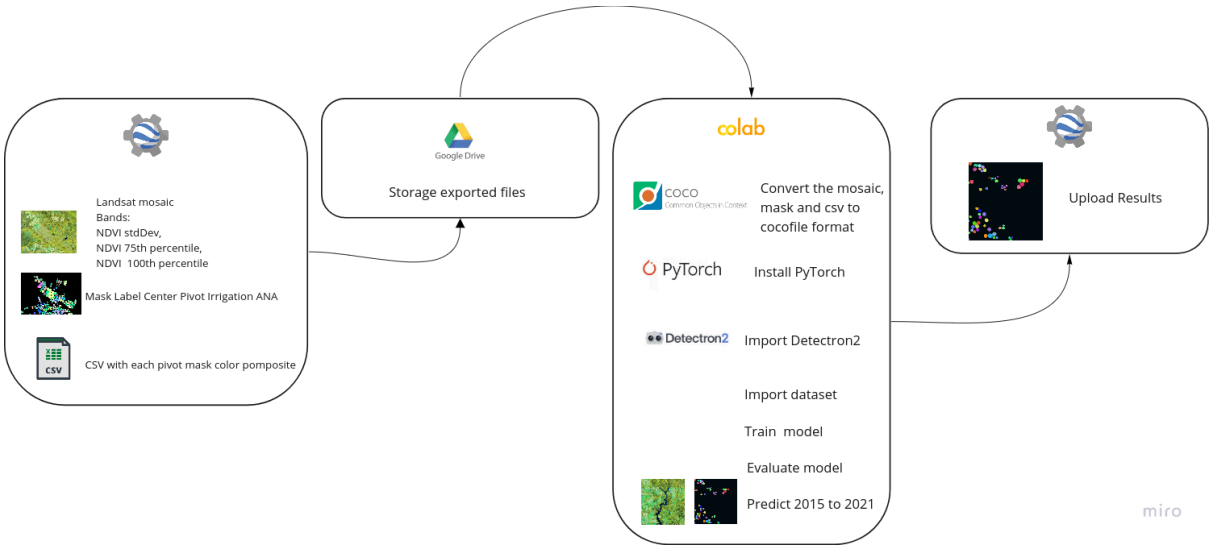


**Figure 20.** Pipeline to use Detectron2 to pivot instance segmentation.

#### 4.8.4 Post-Classification

Post processing of the center pivot irrigation has two more steps besides the spatial and temporal filters, which are focused for solving pivots ‘union’ and ‘edge’ problems.

#### 4.8.4.1 Pivot overlaping

Union problem consists of a false pivot generated between real pivots that are overlapping. Figure 21 exemplifies this problem as well as its resolution.

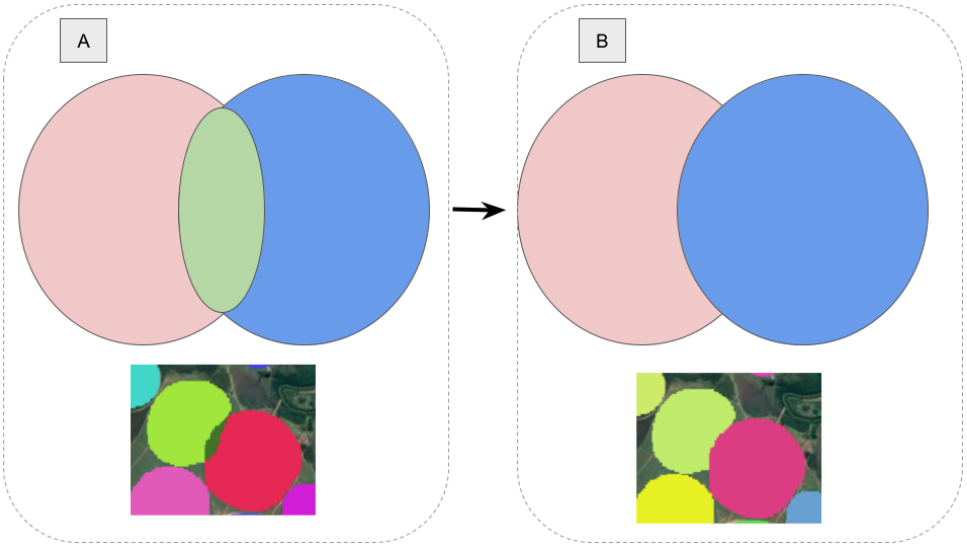


**Figure 21.** Illustration of the problem of the union between two or more center irrigation poles. A) union problem; B) result of the filter applied to solve the union problem.

To solve this union problem it is necessary to find the ID of the false pivot (generated by union of two or more pivots through a sum of true IDs), and then identify the IDs pivots that generated this false pivot ID. Based on this information it is possible to replace a false ID to a true ID, from one of pivots that generated this false ID.

#### 4.8.4.2 Edge Problem

The edge problem is a result of the shape and size of the RCNN Mask input. Some pivots will inevitably be "cut off" due to the size of the input tiles, i.e. one part of the pivot will be in one block (tile) and the other part will be in another adjacent block. The edge problem was solved with the application of two complementary filters (erosion and dilation) and a reduction by spatial connectivity. Figure 22 shows an example of an application to solve edge problems (A).

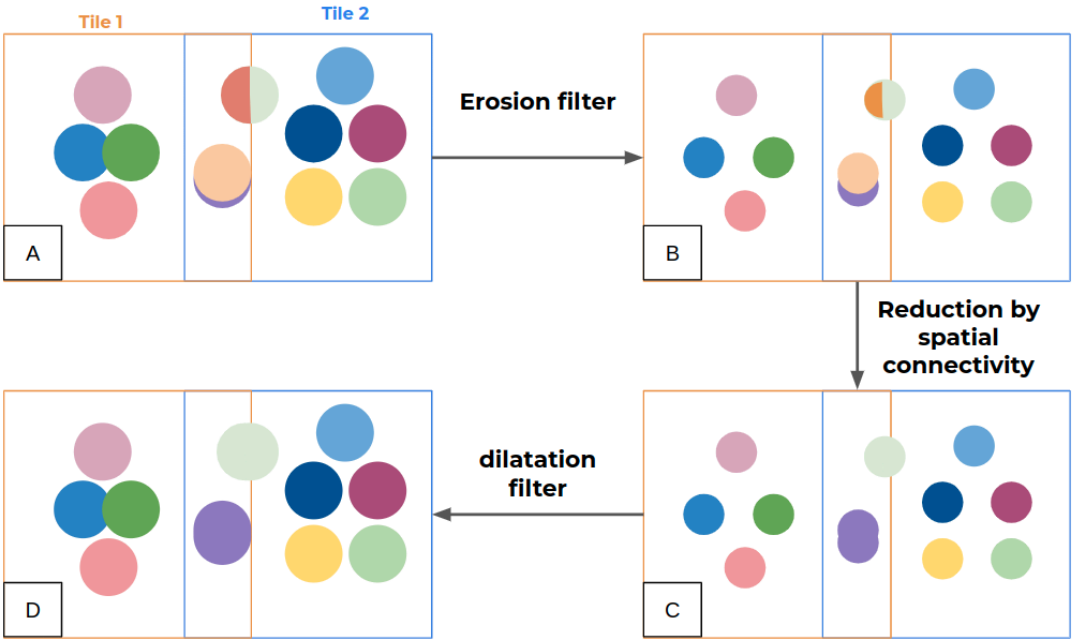


**Figure 22.** A) Example of application of morphological filter to solve edge problems. A) tiles with pivot edge problems; B) erosion filter; C) spatial connectivity Reduction and D) dilatation filter.

The erosion filter is applied to the tiles in order to reduce the size of the instances (pivots) with the goal of isolating them from each other (B). Then, pivots that were "cut off" by the tile of the RCNN Mask and that exist in the overlap of both boundary images are connected (C). Finally, after this step it is necessary to apply the morphological dilation filter to return pivots to their original size (D) .

#### 4.8.4.3 Temporal filter

For temporal consistency of the IDs over time, a temporal filter was applied with the goal that each pivot remains with the same ID over the years. In this step, a reference image was generated through the accumulation function of all years (2015 to 2022), thus the reference image has all the pivots of the time series and their respective IDs. An accumulation of pivots must be calculated for each year, for example, the accumulation of the year 2020 has the pivots of the years 2015, 2016, 2017, 2018, 2019, and 2020.

#### 4.8.4.4 Spatial filter

A spatial filter was used to remove areas smaller than 10 hectares, so that the noise caused by the accumulation function is excluded, as shown in Figure 23.

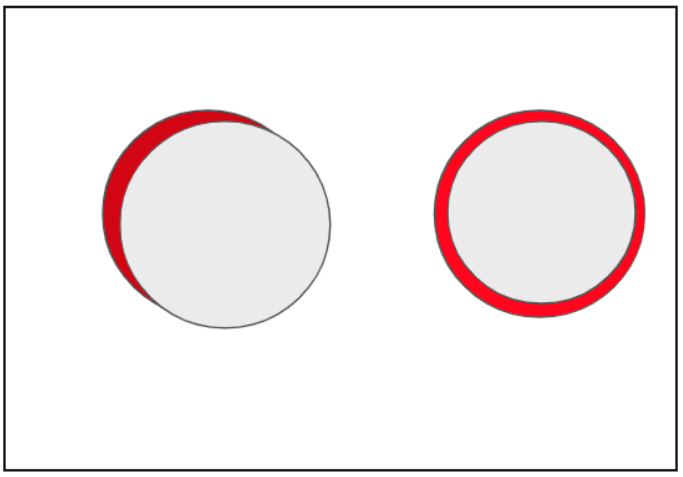

**Figure 23.** Example of spatial filtering. Pivot polygons in red polygon generated by the accumulation function are removed through the spatial filter.

### 4.8.5 Validation strategies

To validate the instance segmentation (Mask RCNN) and semantic segmentation (Unet) methodologies, the Jaccard index was calculated. The Jaccard index (JACCARD, 1901), also known as the Jaccard similarity coefficient or *intersection over union* (IOU), is a statistic used for gauging the similarity and diversity of sample sets and is defined as the size of the intersection divided by the size of the union of the sample sets (Figure 24).

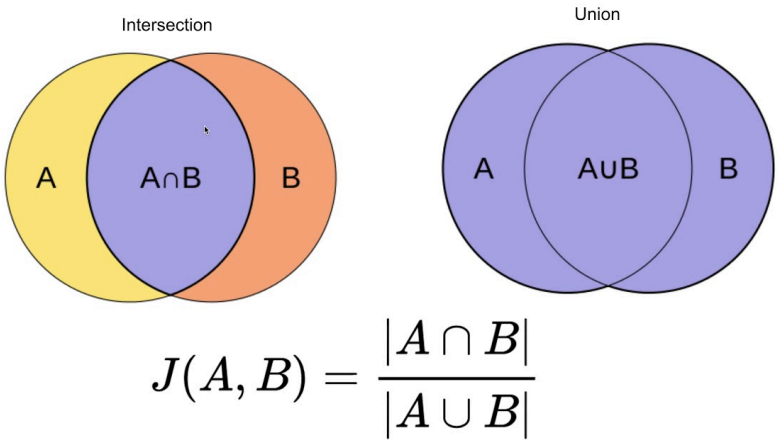


**Figure 24**: Index Jaccard (IOU) calculation.

The spatial similarity of the Unet results with the Mask RCNN results obtained for the year 2019 was 61.7%. The location data of the center pivots of public irrigation by ANA showed 63.1% similarity with the results obtained from the RCNN Mask. The similarity between ANA and Unet data was 78.4%. It is important to note that instance segmentation is a new methodology that is still under development.

### 4.8.6 Results

Mask RCNN returns as output a raster of the input mosaic size (15 x 15 km) composed of 0, which corresponds to no detection of center irrigation pivots and values corresponding to the ID of the classified pivots. Figure 25 shows the input and output of the RCNN Mask prediction.

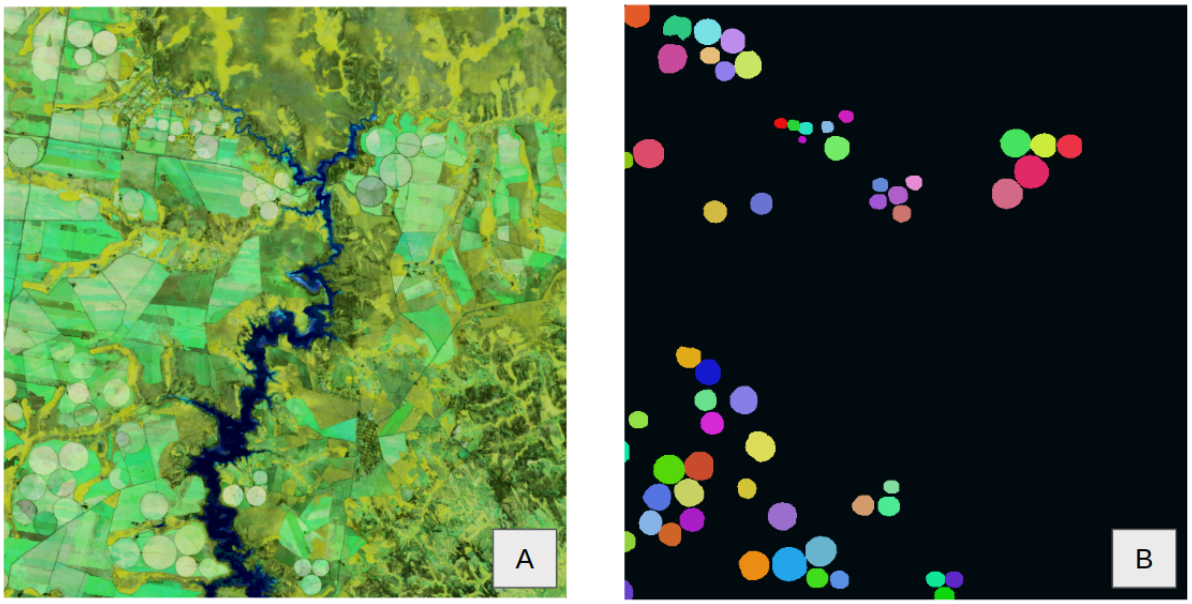


**Figure 25.** Result of the Mask RCNN prediction.

## 4.9 Center Pivot Information

Crop and environmental characteristics of center pivot irrigation were obtained to each individual pivot. Thus, using the geometry of each pivot, the following information was extracted: *i*) crop cycles number of each pivot; *ii*) start and end dates of each cycle; *iii*) crop cycle length in days of each cycle; and *iv*) daily average precipitation of each cycle. Besides this, it was also possible to obtain the information if the pivot was in a perennial cultivation area, and if it did not present internal coherence – due to multiple crops at the same time or complex management – , it was not possible to obtain the previous information (*i*, *ii*, *iii* and *iv*) and the pivot is defined as a non-classified.

### 4.9.1 Image selection

The period used to select the images to obtain a temporal EVI2 curve was based on the crop year. The crop year is different from the conventional year (from January to December), since the crop year aims to define the period when the cultivation occurs in a determined region. Thus, depending on the type of agriculture, the crop year can start in any month of the year, generally following the rainy season, since in this period there is humidity available to the crop development. Thus, to attribute information for each center pivot irrigation, Landsat images (TOA) were selected from a crop year, in order to compute the EVI2 time series.

The crop year was defined automatically for each Landsat scene and year. We defined the crop year as 3 months before and 9 months after the mean vegetative peak month of each scene, based on an EVI2 curve of MODIS observations.

### 4.9.2 Method to attribute information to each pivot

#### 4.9.2.1 Crop cycles number

The first information obtained, that is a base to obtaining the others, was the number of crop cycles of each pivot. An EVI2 curve of Landsat images from the crop year was smoothed to minimize noise and to reconstruct the time series. The Whittaker method (WHITTAKER, 1922) was used to smooth EVI2 temporal series, since this method presents a great alternative to smooth and to reconstruct temporal series, most importantly keeping only meaningful variations and preserving the temporality of them.

Based on the smoothed EVI2 curve, it was possible to identify when inflections occur in the curve, that is, the change of direction of the curve. Thus, it was possible to identify the points of valleys (defined as the inflections of change from negative to positive sign), and peaks (defined as the inflections of change from positive to negative sign) (Figure 26). Finally, to define the number of cycles, this can be counted as the number of peaks (or valleys minus one), determining the number of crop cycles in a period.

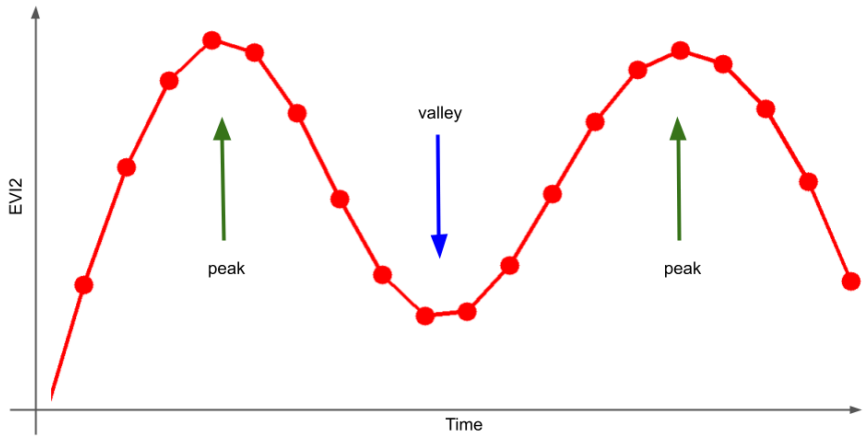


**Figure 26**: Peaks and valleys identification based on the smoothed EVI2 time series curve.

#### 4.9.2.2 Start and end cycles dates

After identifying the peaks and valleys over the EVI2 time series, it was possible to determine the start and end dates of each cycle. In this step we sought to identify the dates of the valley inflections of the EVI2 curve of each pivot. According to the amount of Landsat images available in the crop year, where each one represents a binary information of valley (1) or no-valley (0), it was obtained a percentage of presence of pixels identified as valley (1). Then, after valleys date identification, it was checked if the quantity of them was equivalent to the

expected quantity for the number of cycles of the pivot (number of cycles +1). If this information is true, the pivot is considered well identified, if not, the pivot is considered as non-classified, since due to the internal dynamics it was not possible to identify a spatial coherence in the start and end date definition. This usually occurs for pivots with different crops at the same time.

The valley dates were used as a base to determine start and end cycle dates. Based on the daily interval between the two valleys that compose a cycle, the start date was defined as the $20^{th}$ percentile value, and the end date as the $80^{th}$. This was done to reduce cycle coverage to the period where the crops were active, eliminating soil management periods (JÖNSSON and EKLUNDH, 2004). To avoid omitting the planting period, a -15 days buffer was also added to the start cycle dates.

This cycle delimitation method has some known issues, such as the delimitation of cycles based only on the time value. Improvements in this area will be sought for future collections.

#### 4.9.2.3 Crop cycle length

Crop cycle length in days was obtained as a difference between the end and start date of each pivot for each cycle.

#### 4.9.2.4 Average Daily Precipitation

For Precipitation information we used data from Climate Hazards Group Infrared Precipitation with Stations (CHIRPS) product (FUNK et al., 2015), that provide daily and sub-daily precipitation information for quasi–global spatial coverage (50°S-50°N), from 1981-present, in a 0.05° x 0.05° of spatial resolution. Based on CHIRPS data, an accumulation precipitation of each pivot was obtained and then this amount of precipitation was divided by the number of the days of each cycle, resulting in an average daily precipitation per cycle.

#### 4.9.2.5 Additional Information

In addition to the number of crop cycles, start and end dates, and precipitation information, the product also provides additional information about non-classified, perennial and sugarcane pivots.

Perennial and sugarcane pivots were identified using the respective maps from MapBiomas Collection 9, since cycles and environmental information were only accounted for temporary crop pivots.

Pivots in which it was not possible to identify the start and end dates of each cycle were set as non-classified. This problem can be due to a number of factors. For instance, pivot internal crop dynamics, when there are multiple crops on a single pivot, or the same type of crop, however at different times. There is also the possibility of errors inherited by the individualization of pivots methodology, since a not well-defined geometry may encompass

other land uses or surrounding crops. In these situations, it was not possible to identify coherent start and end dates, since there is no agreement inside the pivot geometry. Figure 27 presents some examples of when it is possible to identify start and end dates and when this identification is not possible, resulting in non-classified pivots.

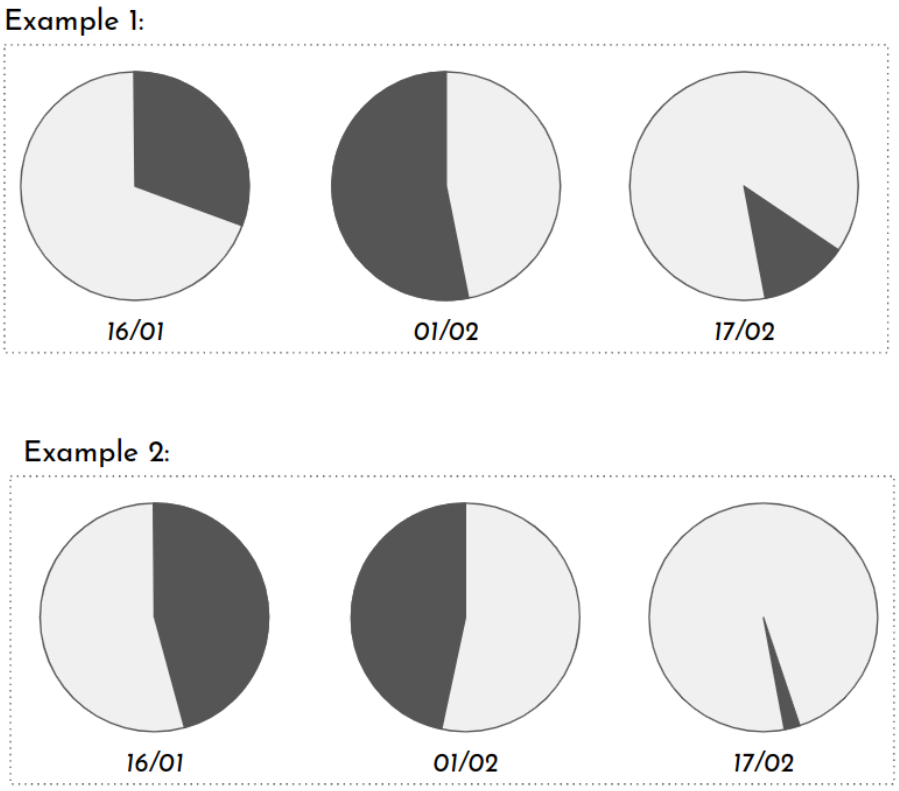


**Figure 27**: Examples of start and end dates identification, and limitations that cause non-classified pivots.

Example 1 shows a pivot in three different Landsat dates. The shaded area represents the area identified as a valley date. In the first image (16/01) there are approximately one quarter of the pivot identified as a valley. This amount is even less in 17/02. However, in the second date (01/02), most of the pivot was identified as a valley, providing a valley date information.

Example 2, on the other hand, presents a more complex situation. In these three dates (16/01, 01/02, and 17/02), there is not a single image where most of the pivot is identified as valley. In this situation there is no possibility to obtain start and end dates by the same method as before (statistical mode), so pivots in this or similar situations were set as non-classified. This is a known flaw in the methodology and improvements will be sought in future collections.

### 4.9.3 Validation strategies

From the total of classified pivots, 250 were randomly selected and evaluated year by year, visually, in order to validate the consistency in terms of class, start and end dates of each cycle, and also the consistency of number of cycles. This total (250) represents between 3 to 6% of total pivot amount, depending on the year, since the number of pivots increases over the years.

The following errors were considered: (1) cycle number errors, when a pivot shows a difference between the number of cycles identified in the methodology and the visual analysis; (2) dates errors, when the pivot has at least one cycle where the start and end dates are not consistent with the expected in the vegetation index curve; (3) class errors, where the pivot was misclassified in any way. The first two errors can occur at the same time, and when so it is likely that the pivot was mostly not well defined. However, the errors individually do not indicate that the pivot is entirely wrong. Class errors can be associated with an omission from the sugarcane and perennial masks. Cycle number and date errors individually show that a cycle in the pivot was misidentified in some way, but not necessarily all of its cycles. Figure 28 presents the rates (%) of pivot without any kind of error, with only one error and with two errors.

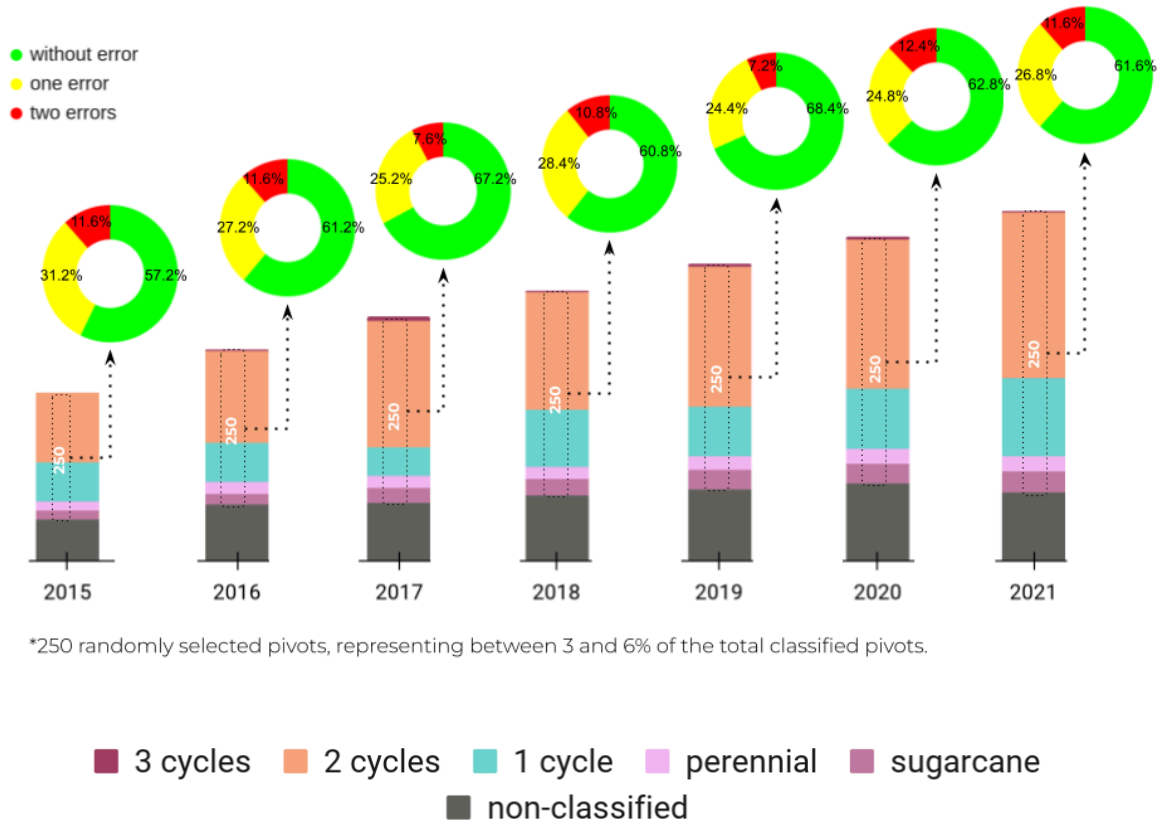


**Figure 28**: Percentage of pivots without errors, with only one error and with two errors identified in 250 pivots selected randomly.

The results presented in the Figure 28 above, show that about 57.2 to 68.4% of pivots randomly selected have none of the analyzed errors, while around 24.4 to 31.2% of samples presented only one error, and 7.2 to 12.4% of data evaluated presented two types of errors. The analysis also provides information about the type of these errors identified. Figure 29 presents the error rates identified by the pivots sample randomly selected.

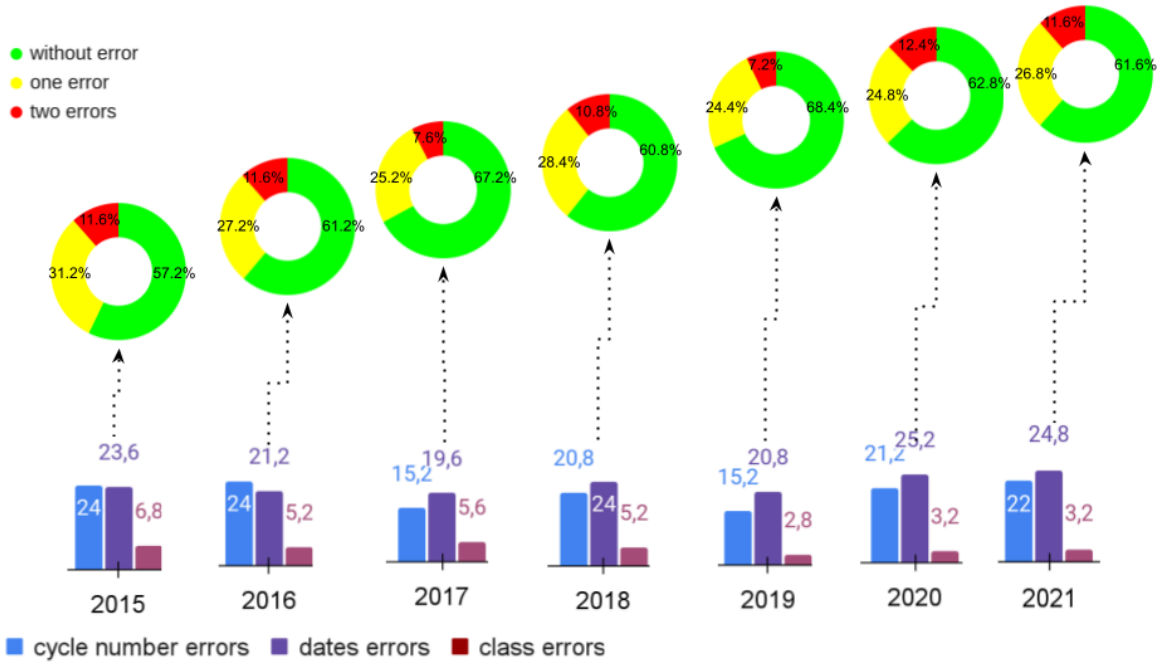


**Figure 29**: Percentage of type of errors identified in 250 pivots selected randomly.

Figure 29 informs us that we have two main types of errors on pivots. For instance, errors due to incorrect cycle accounting are about 15 to 25% of the errors identified. About 19.6 to 25.2% of errors are related to errors in identifying the start and end dates of cycles, and less than 7% of errors are related to errors in pivot class, i.e. classification of the type of use and coverage of that pivot.

### 4.9.4 Results

The results presented in Figure 30 highlight the example of the expansion, and intensification of the agriculture through the irrigation over Minas Gerais, showing the number of pivots, for each year, with 1, 2 and 3 cycles.

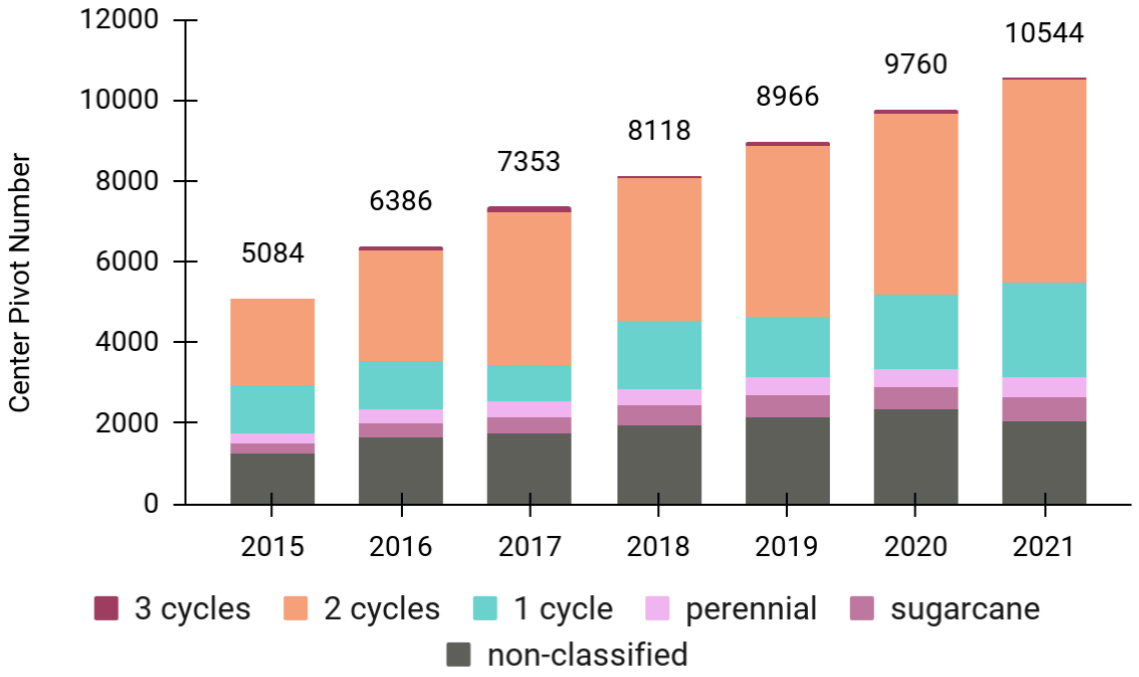


**Figure 30**: Number of center pivot irrigation with one, two and three cycles, perennial, sugarcane and non-classified in Minas Gerais state.

Overall, in Brazil, 19% of center pivot irrigation has one crop cycle, while 46% present two crop cycles, and approximately 1% were cultivated three times over the analyzed years (2015-2022). In addition, approximately 24% of center pivot irrigation was not classified as a function of methodology limitation. Around 6% of these pivots were identified as perennial pivots and 5% as sugarcane.

In addition to this information on the expansion and intensification of agriculture, in terms of the number of gullies, some other information on the dynamics of gullies can also be obtained from this product. For example, for the state of Minas Gerais, some general information about the region's crop dynamic was summarized. It was possible to identify the months of start and end cycle, the number of days of each cycle and how much precipitation occurred in this period, also to each cycle. Figure 31 presents a temporal average of this information for the pivots identified with crop dynamics (pivots with 1, 2 or 3 cycles), in the Minas Gerais state.

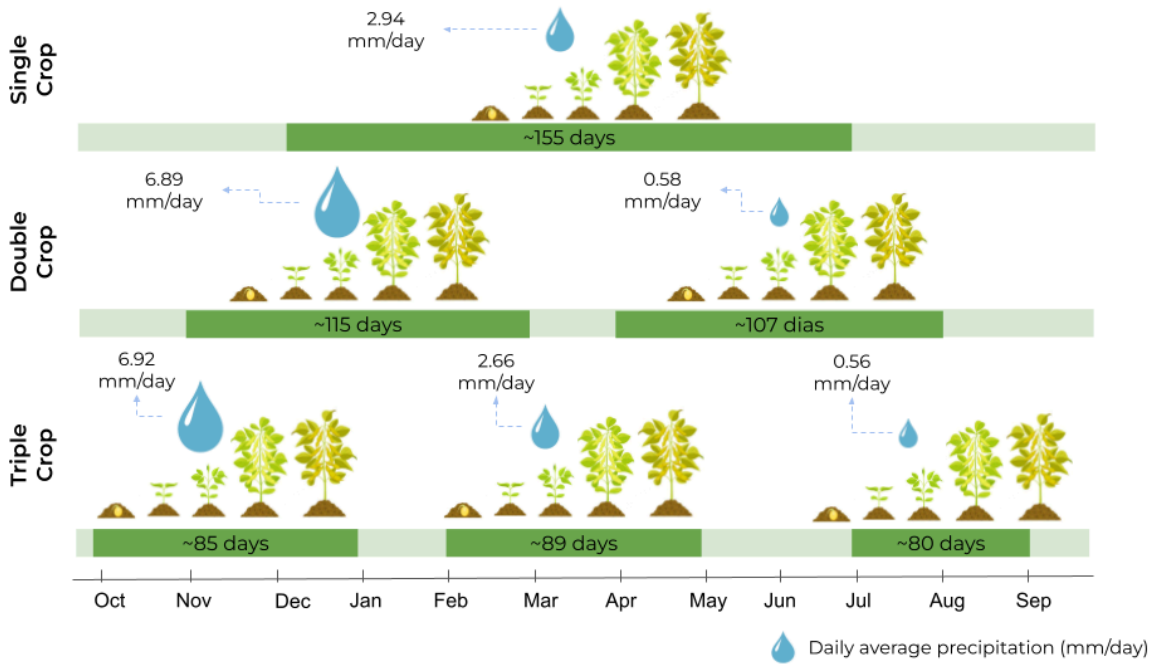


**Figure 31**: Summary of pivot dynamics for Minas Gerais state.

In Figure 31 presented above, it is possible to see that both the start and end months of each cycle, as well as its duration and daily average precipitation varies according to the number of times the pivots have been cultivated in the year.

For instance, on pivots with one single crop cycle, the cultivation usually starts in December with a harvest occurring around July. Pivots with only one cycle present a longer cycle duration, of approximately 155 days,. The daily precipitation is about 2.94 mm/day, since the cycle also extends over rainy (December, November, January and February, June and July) and dry (May, June and July) months in this region.

For pivots that present a double-crop there is a different dynamic. In these pivots the cycle duration is around 115 days for the first cycle and around 107 days for the second cycle. Comparing pivots with single and double-crops it is possible to verify that for double-crop pivots the period when the cultivation occurred was usually earlier than the single-crop pivots, with planting starting around November and harvesting around March. As this first cycle of the double crop pivots is concentrated in the rainiest months of this region, the daily average precipitation is higher, around 6.89 mm/day. Regarding the second cycle of double-crop pivots, this usually starts planting around April and harvesting usually occurs in August. Because it comprises mainly the winter months, this period presents low precipitation, with a rate of approximately 0.58 mm/day, indicating that only the precipitation of the period is not sufficient for the development of the crop, requiring the use of an irrigation system for this second harvest.

For pivots with triple-crop, the crop duration is even shorter than pivots with one or double-crops. In these pivots with triple-crops, generally the cycles extend from from 80 to

89 days. In addition, the period of cultivation of the first cycle starts earlier than pivots with single or double-crops, starting in October and the harvest occurring in January. The second cycle normally starts in February and the harvest occurs in May, while the third cycle extends from July to September. The first two cycles of triple-crop pivots take place at least partially in the region's rainy season, with a rate about 6.92 mm/day for the first cycle and 2.66 mm/day for the second cycle, indicating a lower dependency of the irrigation system in the first cycle compared to the second one. However, during the third cycle precipitation rate is about 0.56 mm/day, suggesting a significant increase of irrigation importance for crop development.

## 5 References


Abatzoglou, J. T., Dobrowski, S. Z., Parks, S. A., & Hegewisch, K. C. (2018). TerraClimate, a high-resolution global dataset of monthly climate and climatic water balance from 1958–2015. *Scientific data*, *5*(1), 1-12.

AGÊNCIA NACIONAL DE ÁGUAS (ANA). Atlas irrigação: uso da água na agricultura irrigada /Agência Nacional de Águas. Brasília: ANA, 2017.

AGÊNCIA NACIONAL DE ÁGUAS (ANA). Levantamento da agricultura irrigada por pivôs centrais no Brasil/Agência Nacional de Águas, Embrapa Milho e Sorgo. 2. ed. Brasília: ANA, 2019a.

AGÊNCIA NACIONAL DE ÁGUAS (ANA). Levantamento da cana-de-açúcar irrigada e fertirrigada no Brasil/Agência Nacional de Águas. 2. ed. Brasília: ANA, 2019b.

AGÊNCIA NACIONAL DE ÁGUAS (ANA). Polos nacionais de agricultura irrigada: mapeamento de áreas irrigadas com imagens de satélite/Agência Nacional agricultura irrigada por pivôs centrais de irrigação no Brasil - 1985 - 2022/ Agência Nacional de Águas - Brasília: ANA, 2022. Boletim do SNIRH n. 4.

AGÊNCIA NACIONAL DE ÁGUAS (ANA). Levantamento da /Agência Nacional de Águas - Brasília: ANA, 2020.

AGÊNCIA NACIONAL DE ÁGUAS (ANA). Atlas irrigação: uso da água na agricultura irrigada (2ª edição)/Agência Nacional de Águas - Brasília: ANA, 2021a.

AGÊNCIA NACIONAL DE ÁGUAS (ANA). Mapeamento do arroz irrigado no Brasil/Agência Nacional de Águas, Companhia Nacional de Abastecimento. Brasília: ANA, 2021b.

Breiman, Leo. Random forests. Machine learning, v. 45, n. 1, p. 5-32, 2001.

EMPRESA BRASILEIRA DE PESQUISA E AGROPECUÁRIA (EMBRAPA). Dados conjunturais da produção de arroz (Oryza sativa L.) no Brasil (1986 a 2019): área, produção e rendimento. Santo Antônio de Goiás: Embrapa Arroz e Feijão, 2020. Available at: <http://www.cnpaf.embrapa.br/socioeconomia/index.htm>. Access on : 07/04/2022.

INSTITUTO BRASILEIRO DE GEOGRAFIA E ESTATÍSTICA (IBGE). 2009. Censo agropecuário 2006: resultados definitivos. Rio de Janeiro: IBGE, 2009.

INSTITUTO BRASILEIRO DE GEOGRAFIA E ESTATÍSTICA (IBGE). 2019. Censo agropecuário 2017: resultados definitivos. Rio de Janeiro: IBGE, 2019.

Deines, J. M., Kendall, A. D., Crowley, M. A., Rapp, J., Cardille, J. A., & Hyndman, D. W. (2019). Mapping three decades of annual irrigation across the US High Plains Aquifer using Landsat and Google Earth Engine. Remote Sensing of Environment, *233*, 111400.

Farr, T.G., Rosen, P.A., Caro, E., Crippen, R., Duren, R., Hensley, S., Kobrick, M., Paller, M., Rodriguez, E., Roth, L., Seal, D., Shaffer, S., Shimada, J., Umland, J., Werner, M., Oskin, M., BURBANK, D., and Alsdorf, D.E. (2007). The shuttle radar topography mission: Reviews of Geophysics, v. 45, no. 2, RG2004, at <https://doi.org/10.1029/2005RG000183>.

Funk, C., Peterson, P., Landsfeld, M., Pedreros, D., Verdin, J., Shukla, S., ... & Michaelsen, J. (2015). The climate hazards infrared precipitation with stations—a new environmental record for monitoring extremes. *Scientific data*, *2*(1), 1-21.

Gao, B. C. (1996). NDWI—A normalized difference water index for remote sensing of vegetation liquid water from space. *Remote sensing of environment*, *58*(3), 257-266.

Jaccard, P. (1901). Étude comparative de la distribution florale dans une portion des Alpes et des Jura. *Bull Soc Vaudoise Sci Nat*, *37*, 547-579.

Jiang, Z., Huete, A. R., Didan, K., & Miura, T. (2008). Development of a two-band enhanced vegetation index without a blue band. *Remote sensing of Environment*, *112*(10), 3833-3845.

Jönsson, P., & Eklundh, L. (2004). TIMESAT—a program for analyzing time-series of satellite sensor data. *Computers & geosciences*, *30*(8), 833-845.

Nagler, P. L., Inoue, Y., Glenn, E. P., Russ, A. L., & Daughtry, C. S. T. (2003). Cellulose absorption index (CAI) to quantify mixed soil–plant litter scenes. Remote Sensing of Environment, 87(2-3), 310-325.

Ronneberger, O.; Fischer, P.; Brox, T. (2015). U-Net: Convolutional networks for biomedical image segmentation. In International Conference on Medical Image Computing and Computer-Assisted Intervention; Springer: Berlin, Germany, 2015; pp. 234–241.

Rouse, J., Haas, R., Schell, J., & Deering, D. (1974). Monitoring vegetation systems in the great plains with ERTS. In *Proceedings of the Third Earth Resources Technology Satellite—1 Symposium; NASA SP-351* (pp. 309-317).

Saraiva, M., Protas, É., Salgado, M., & Souza Jr, C. (2020). Automatic Mapping of Center Pivot Irrigation Systems from Satellite Images Using Deep Learning. Remote Sensing, 12(3), 558.

Whittaker, E. T. (1922). On a new method of graduation. *Proceedings of the Edinburgh Mathematical Society*, *41*, 63-75.

Xu, H. (2006). Modification of normalized difference water index (NDWI) to enhance open water features in remotely sensed imagery. *International journal of remote sensing*, *27*(14), 3025-3033.